Halo-coronal mass ejections near the 23rd solar minimum: lift-off, inner heliosphere, and in situ (1 AU) signatures

D. B. Berdichevsky, C. J. Farrugia, B. J. Thompson, R. P. Lepping, D. V. Reames, M. L. Kaiser, J. T. Steinberg, S. P. Plunkett, D. J. Michels

Annales Geophysicae (2002) 20: 891–916 © European Geophysical Society 2002

Annales Geophysicae

Halo-coronal mass ejections near the 23rd solar minimum: lift-off, inner heliosphere, and in situ (1 AU) signatures

D. B. Berdichevsky[1, 3], **C. J. Farrugia**[2], **B. J. Thompson**[3], **R. P. Lepping**[3], **D. V. Reames**[3], **M. L. Kaiser**[3], **J. T. Steinberg**[4, 7], **S. P. Plunkett**[5, 6], **and D. J. Michels**[6]

[1]Emergent Information Technologies-East, Largo, MD 20774, USA
[2]Space Science Center, University of New Hampshire, Durham, NH, USA
[3]NASA/Goddard Space Flight Center, Greenbelt, MD 20771, USA
[4]Center for Space Research, MIT, Cambridge, MA, USA
[5]USRA, at Naval Research Laboratory, Washington, D. C. 20735, USA
[6]Naval Research Laboratory, Washington, D. C. 20375, USA
[7]now at: Los Alamos Nat. Lab., NM, USA

Received: 1 October 2001 – Revised: 3 March 2002 – Accepted: 10 March 2002

Abstract. The extreme ultraviolet (EUV) signatures of a solar lift-off, decametric and kilometric radio burst emissions and energetic particle (EP) inner heliospheric signatures of an interplanetary shock, and in situ identification of its driver through solar wind observations are discussed for 12 isolated halo coronal mass ejections (H-CMEs) occurring between December 1996 and 1997. For the aforementioned twelve and the one event added in the discussion, it is found that ten passed several necessary conditions for being a "Sun-Earth connection". It is found that low corona EUV and Hα chromospheric signatures indicate filament eruption as the cause of H-CME. These signatures indicate that the 12 events can be divided into two major subsets, 7 related to active regions (ARs) and 5 unrelated or related to decayed AR. In the case of events related to AR, there is indication of a faster lift-off, while a more gradual lift-off appears to characterize the second set. Inner heliospheric signatures – the presence of long lasting enhanced energetic particle flux and/or kilometric type II radio bursts – of a driven shock were identified in half of the 12 events. The in situ (1 AU) analyses using five different solar wind ejecta signatures and comparisons with the bidirectional flow of suprathermal particles and Forbush decreases result in indications of a strong solar wind ejecta signatures for 11 out of 12 cases. From the discussion of these results, combined with work by other authors for overlapping events, we conclude that good Sun-Earth connection candidates originate most likely from solar filament eruptions with at least one of its extremities located closer to the central meridian than $\sim 30°$ E or $\sim 35°$ W with a larger extension in latitudinal location possible. In seven of the twelve cases it appears that the encountered ejecta was driving a shock at 1 AU. Support for this interpretation is found on the approximately equal velocity of the shock and the ejecta leading-edge. These shocks were weak to moderate in strength, and a comparison of their transit time with their local speed indicated a deceleration. In contradistinction with this result on shocks, the transit time versus the local speed of the ejecta appeared either to indicate that the ejecta as a whole traveled at constant speed or underwent a small amount of acceleration. This is a result that stands for cases with and without fast stream observations at their rear end. Seven out of twelve ejecta candidate intervals were themselves interplanetary magnetic cloud (IMC) or contained a previously identified IMC. As a by-product of this study, we noticed two good ejecta candidates at 1 AU for which observation of a H-CME or CME appears to be missing.

Key words. Radio science (remote sensing); Solar physics, astrophysics and astronomy (flares and mass ejections); Space plasma physics (nonlinear phenomena)

Correspondence to: D. B. Berdichevsky
(xrdbb@lepvx3.gsfc.nasa.gov)

1 Introduction

Before halo coronal mass ejections (H-CMEs) were first observed, eruptive prominences were known to relate to major Hα-flares (see, e.g. Zirin, 1966; Martin, 1973) and to CMEs (see e.g. Munro et al., 1979) and were suspected of being directly connected to geomagnetic activity (see, e.g. Joselyn and McIntosh, 1981). In their statistical study, Cane et al. (1986) include the solar filament disappearance on 27 November 1979. This event happened to be associated with Howard et al. (1982), who first reported an observation of a H-CME event. This solar event was followed about three days later by moderate to severe geomagnetic disturbances. This view between H-CME and geomagnetic disturbances became established in the scientific community (see, e.g. St. Cyr and Hundhausen, 1988). This was a great achievement considering the difficulties inherent in white light coro-

nagraph detection for an H-CME that propagates along the line of sight, because the scattered light signature (Thomson scattering) favors the plane of the sky. In the past, it was not possible to establish a one-to-one correspondence between the observation of a CME at the Sun and the corresponding transient in the solar wind (hereafter called ejecta); in general, only the brightest or strongest CMEs were noticed (Gosling et al., 1974; St. Cyr et al., 1999 and references therein). The LASCO white-light coronagraph on the SOHO spacecraft, located at 0.01 AU upstream of the Earth, probably observes most H-CMEs thanks to its unique high sensitivity and wide dynamic range (Brueckner et al., 1995). (It is 200 times more sensitive than the SOLWind coronagraph.) LASCO/SOHO is able to discern such minute changes in white light intensities that observation of the steady outflow of coronal material along the solar helmet streamers at several solar radii have been made for the first time (e.g. Sheeley et al., 1997). For the present study this sensitivity is essential. Starting in 1996 the almost continuous access to solar and interplanetary data (by the International Solar Terrestrial Physics (ISTP) program (Acuña et al., 1995) in conjunction with solar observations by Yohkoh, and GOES satellites, and solar ground-based observatories) made it possible to establish the likely connection between the Sun source of an H-CME and specific solar wind structure(s) at 1 AU, in the vicinity of the Earth (see, e.g. Burlaga et al., 1998; Berdichevsky et al., 1998; Gopalswamy et al., 1998; Webb et al., 2000a), thereafter called Sun-Earth connections.

We explored the interval of a relatively simple solar and heliospheric magnetic field organization with mostly well-defined Sun polarity, and a solar neutral line primarily close to the Sun's equatorial line (see, e.g. Michels, 1998; Sanderson et al., 1998). During this time, the Sun had very low "soft X-ray" background radiation, and there was low background in solar energetic particles in the interplanetary medium. In this paper, we present a study, statistical in nature, of a larger set of events, with their source at the front side of the Sun, than the sets investigated in some of the resent statistical studies (Brueckner et al., 1998; Cane et al., 1998; Webb et al., 2000b). We complement those studies with a more detailed analysis of the occurrence of many hours, up to more than two days, of unusual solar wind condition. (Unusual solar wind intervals being the possible manifestation of the presence of ejected material at 1 AU, starting three to five days after the time of observation of an H-CME). Furthermore, we explore the connection of these ejecta with the common observation of a likely driven shock, a consistence element for the testing of the Sun-Earth connection hypothesis. Therefore, it is possible that this work may help to answer a few of the following "simple" questions we may pose after the occurrence of individual Sun front side H-CMEs near the solar minimum. What were the EUV low Sun corona transient signatures? How often were we able to relate an ejecta with the H-CME? If it was possible to relate an ejecta at 1 AU with the H-CME, how often was it possible to infer the presence of the ejecta along its route away from the Sun, before arriving to the in situ observation at 1 AU? What were the most frequently observed characteristics of these transients at 1 AU? How do their transit times relate to their observed speed at 1 AU?

Included in the study is each possible Sun-Earth connection that may be linked to a candidate H-CME originating on the front side of the Sun (e.g. St. Cyr et al., 2000; LASCO CMEs web public list of CMEs with URL: http://lasco-www.nrl.navy.mil/ cmelist.html), and separated in time by at least three days from any other front side H-CME, observed from December 1996 to December 1997.

The layout of the paper is as follows. In Sect. 2, we give a short description of instrumentation and data sets. Section 3 outlines our selection criteria of the candidate Sun-Earth connection. Their main signatures in chronological order from the Sun, through the inner heliosphere and the in situ solar wind observations at 1 AU are analyzed statistically in Sect. 4. Section 5 presents a discussion and comparison of these results to work done by other authors. Conclusions are drawn in Sect. 6.

2 Data sets and instrumentation

The monitoring of the solar corona with LASCO was combined with an equal amount of solar disk observation with the EUV images of the Repetitive Extreme-Ultraviolet Imaging Telescope EIT on SOHO (Delaboudinière et al., 1995). At the same time, instrumentation on Wind provided uninterrupted coverage of the solar wind conditions at 1 AU. Radio emission and energetic particle detectors on Wind allowed us to infer the presence of the interplanetary (IP) shocks, driven by a transient (ejecta). In this way, a statistical study of the possible source, motion and 1 AU signatures of the Sun-Earth connection candidate events can be performed. The continuous flow of space data was made possible through the combined effort of the Deep Space Network and the ISTP Ground System including the Central Data Handling Facility (Mish et al., 1995).

Observations of the low corona include iron line images (171, 195, 284, 304 Å) with the SOHO/EIT instrument, X-ray images with the thermal X-ray instruments on Yohkoh/Soft X-ray Telescope, and spectrograms showing decametric type II and III radio emissions with the WAVES/Wind instrument. The observation of the integrated solar X-ray flux in the wavelength range 1–8 Å is from the publicly available STX instrument data from the environmental GOES satellites (internet web address with URL: http://sec.noaa.gov/ftpmenu/indices.html). In addition, when available, we complement a time line for each event with input from reports on chromospheric observations (from Hα line observation and metric radio bursts, as published in the Solar Bulletin, and other sources (see, e.g. Webb et al., 1998; Hudson et al., 1998; Webb et al., 2000b), or made available through private communication (Prestage, Culgoora, Australia, 1999; Mann, Potsdam, Germany, 1999).

Inferences about driven shocks in the inner heliosphere are made from (a) energetic particles observations with the

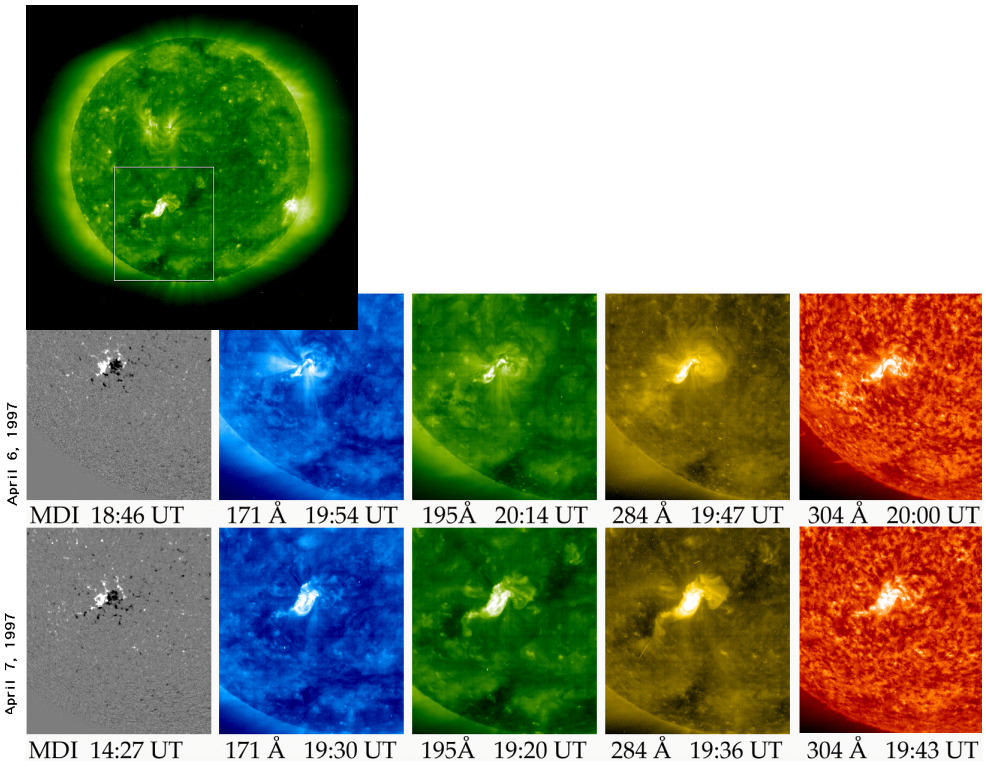

Plate I: A composite showing: full image of the Sun on 195 Å Fe XII line (After halo-CME, Event 5). The bright new arcade formation, enclosed by the white box is at AR 8027. White box region in top image is seen from left to right in two rows of images. The first column of images shows some evolution at photospheric level (magnetogram; Scherrer et al., 1995), and in the following columns stronger evolution (typical arcade formation after the lift-off as well as dimming regions in the lower row) for the ions Fe IX-X, Fe XII, Fe XIV light wave-lengths 171, 195, 284. Dimming and arcade formation is less noticeable in the He II 304 Å light line.

EPACT/Wind instrument (von Rosenvinge et al., 1995), and (b) Decametric to Kilometric radio bursts detected with the WAVES/Wind instrument. WAVES/Wind (Bougeret et al., 1995) is a very sensitive instrument, capable of locating the spatial origin of radio emissions in the three-dimensional heliosphere.

The in situ observations of the interplanetary magnetic field (IMF) and the solar wind plasma parameters (temperature, density and bulk flow speed of electrons and protons, and He^{++}/H^{+} relative abundance) were acquired by the high accuracy instruments MFI (Lepping et al., 1995) and SWE (Ogilvie et al., 1995) on Wind. The moments used in this analysis are $\sim$15-sec averages, spaced every 46 or 92 s, of the solar wind H^{+} and He^{++} distribution, and 1-min averaged magnetic field vectors.

3 Selection criteria and signatures

The set of H-CMEs is composed of wide angle events as observed in the coronograph (though it does include a few events less wide than 360° that extend from above one of the Sun poles to the other hemisphere beyond the solar equatorial line) as observed from the Earth. St. Cyr et al. (2000) gives detailed arguments on this and other classification criteria for these LASCO/SOHO CMEs.) The timing of each H-CME corresponds to the appearance in the field of view of the LASCO/SOHO C2-coronograph.

On images of the Sun, for each candidate H-CME, we review changes that occur before and after the H-CME is observed, as illustrated in Plate I, which shows examples of dimming and new arch-formation after the H-CME. Dimming regions and new arcade formation give an indication of the approximate extent and location of the source region on the disk. In a sequence of EIT EUV iron line images, the occurrence of rising loops, near the limb, may represent the reformation of a new arcade over a channel that contained an erupted filament. In a few cases, EIT did not operate through the time of interest and we searched for sigmoid loop disappearance observed with the Yohkoh STX experiment, and the report of Hα filament disappearance by solar observatories (printed and/or on-line Solar Bulletins, e.g. at the web site with URL: http://sec.noaa.gov/ftpmenu/indices. html). Within hours of the timing of the CME, we checked for the occurrence of a GOES soft X-ray enhancement, and the detection of metric radio bursts at the time of the observation.

In some cases, the appearance of a EIT-wave, on image-differences of the Sun (shown in Plate IIa), may be a better way to determine the time of the rising of the CME through the low corona (see, e.g. Thompson et al., 1998, 1999a). The EIT wave's center, from which it tends to spread over the

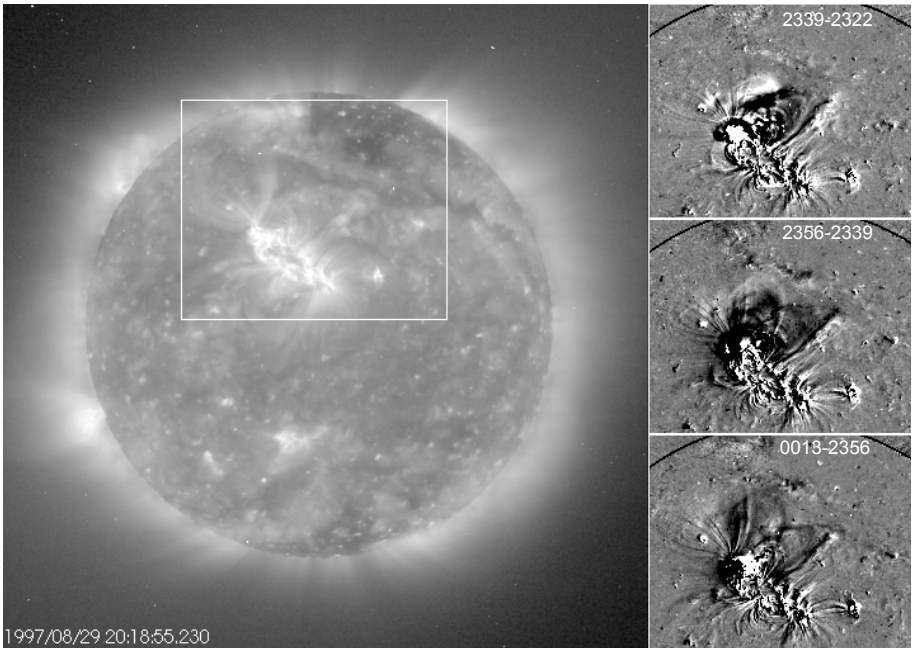

Plate IIa: Sun low corona UVI 195 Å iron-line image at 18:55 UT on 29 August 1997 with AR enclosed in white box, Event 12. The sun disk enclosed by the white box appears on the right. On the right, from top to bottom, panels order image differences chronologically, illustrating the advance on the low corona of the EIT-wave (changing location white and dark areas).

solar surface, suggests the heliographical source location of the CME (see Plate IIa). It usually appears to be close to the location of an eruptive optical Hα flare (Solar Bulletin reports). Its occurrence in time seems to coincide with Type II decametric radio bursts (see, e.g. Reiner et al., 1998a; Berdichevsky et al., 1998; Thompson et al., 1998). It may be a manifestation in the low corona of the chromospheric blast-waves known as Moreton waves, also identified as associated with the lift-off of the CME (Pintér, 1977; Neupert, 1989; Uchida, 1968, 1973).

In other cases the prime evidence of a front side H-CME is the EUV series of images showing a filament eruption, the equivalent to a prominence eruption (see, e.g. Thompson et al., 1999a, b). In a succession of two-dimensional EIT images, a dark filament eruption (an EUV absorption feature) may appear as a filament that increases in size and width, and shifts the location away from its original location until its image becomes vague (it disappears) at the time, on or before the H-CME is observed. An example is given in Plate IIb. At 23:40 UT, the black arrow in the top image shows the filament erupting. Before, at 22:26 UT, a black arrow in the central image indicates a dark quiescent filament located approximately between E 13 N 39 and W 4 N 20 on the low corona, in the 195 Å iron light full image of the Sun. This filament starts its eruption at 22:30 UT on 27 September 1997. This image of the filament is presented at same scale in the bottom left panel (notice here the black arrow's head ending just on top of the filament). After the start of the eruption, the middle bottom image shows two changes at 23:57 UT. A shifted, broader, nearly translucent, and elongated shadow is one feature indicated with the black arrow. It is a stage in the evolution of the filament eruption. The other new feature is an arcade formation starting on the left of the middle bottom panel, with its most recent bright loop shown with a white arrow. In the right bottom panel, the white arrow at 01:51 UT, on the next day points to a more advanced stage of the arcade formation process at the time that the H-CME is in the field of view of the LASCO/SOHO coronograph (not shown). Also, it appears to be dimming to the left of the new arcade formation, in the right bottom panel. A coronal filament eruption seems to belong to the same type of signature as the chromospheric observation of filament eruption in Hα. A long filament, many degrees in extension on the face of the Sun, may take a long time to erupt. This was the case with the 7 February 1997 prominence and filament eruption (Gopalswamy et al, 1998), and possibly the one on 17 September 1997. In most cases, the low corona EUV signatures of a halo CME involve a large amount of spatial motion in EIT-wave and filament eruption. This is to a lesser extent the case with rising loops.

We inferred the possible presence of the ejected material in the inner heliosphere, and sometimes beyond 1 AU, from the monitoring of kilometric Type II radio bursts and MeV EP observed between the time of the H-CME and the passage of the driven shock through the Earth's orbit. Figure 1 presents an example of these signatures. On the left side of the top panel, the Type III radio bursts appear as solid red, because their high intensity saturates the color scale selected

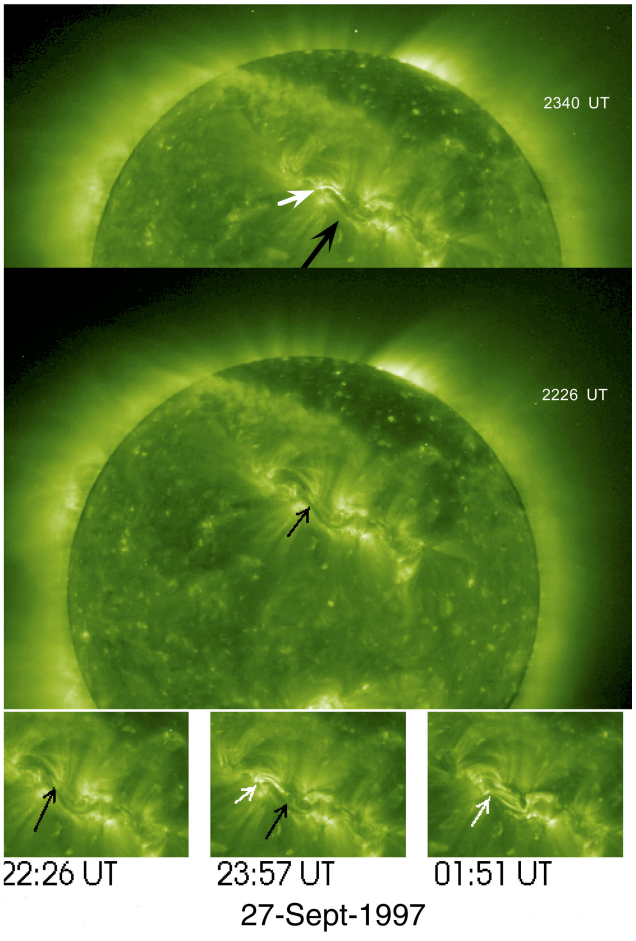

Plate IIb: In the middle image of the Sun (UVI 195 Å iron line) the black arrow shows filament and filament channel before eruption (22:26 UT, on 27 September 1997, Event 14). The black arrow in top image shows the enlarged, shadow-like shape of the erupted filament, and the white arrow points to a bright new arcade formation (23:40 UT). Bottom, from left to right the sequence shows in the right panels a more advanced stage of eruption at 23:57 UT on 27 September, and the long arcade formation created after filament eruption, at the time of the halo-CME (∼ 01:50 UT, 28 September).

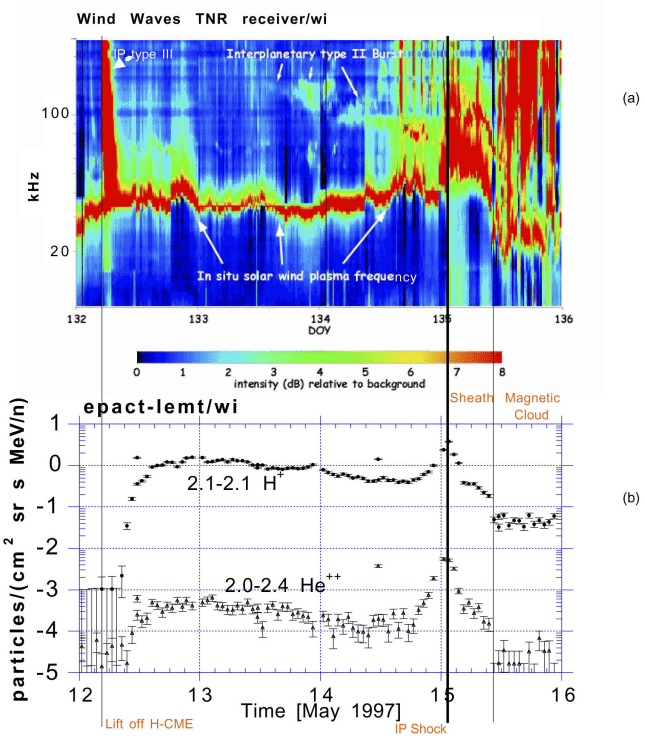

Fig. 1. Top panel shows radio frequency spectrogram (10–400 kHz) from start to end of Event 9. The color scale is chosen to highlight weak Type II radio bursts (top arrows on 13 and 14 May 1997). Solid red radio emissions on the left are Type III radio bursts that mark the approximate start of the event at the Sun. The start of the right, low wave enhancements (below plasma line) marks the time of the passage of the shock on 15 May 1997. Bottom panel shows on the left the rise of the energetic particle (EP) fluxes, indicating the start of the EP gradual event. The EP spike marks the shock passage on 15 May 1997 and the second flux dip, on the right, indicates the starting time of the passage of the interplanetary magnetic cloud (IMC) at Wind.

to highlight the much weaker and slowly drifting Type II radio bursts. These kilometric Type II radio bursts are the continuation of the metric and decametric radio emissions near the surface of the Sun (not shown) and are indicative of the advance of the IP shock into the interplanetary medium (Reiner et al., 1998b). The fundamental Type II radio emission reaches the value of the in situ plasma frequency at the time the shock is observed at ∼ 1 AU, near Earth, on 15 May 1997. The intense low-frequency excitations downstream of the shock are trapped electromagnetic plasma waves, possibly the local source of the Type II radio bursts (Lengyel-Frey et al., 1997; Thejappa et al., 1998). More intense radio emissions, above the plasma frequency, are in part a consequence of currents generated by turbulence in the "sheath" region between the shock and the ejecta. Other sources of intense radio emissions observed by Wind/WAVES behind the shock are of terrestrial origin. Aurora kilometric radio (AKR) emissions occur in response to the intense, fluctuating southward-oriented IMF, and they persist through 15 May. The bottom panel in Fig. 1 shows the rise above the background level of the 1–2 MeV particles, energized at the shock and observed at 1 AU, a few hours after the lift-off of the CME on 12 May. The approximately steady flux following their rise, and lasting until further enhancement closer to the in situ observation of the shock, is interpreted as a typical EP time profile of a shock moving in a direction approximately radial from the Sun. This is consistent with the central location on the solar disk of this event. Finally, the spike-like enhancement of the MeV EP fluxes, beginning before the start of 15 May indicate the proximity of the IP shock. Following the shock, the two-step decrease in these MeV EPs appears to be the result of shielding by strong magnetic fields, first in the sheath region and then in the ejecta time interval. This is consistent with the Earth being engulfed by an interplanetary magnetic cloud

Table 1. Synoptic time-line of the Sun source of H-CME and the possible ejecta manifestations at 1 AU

No.	H-CME	Signatures				
	date and time M/D/Y UT	on Sun (time in UT)	Shock remote sensing Date (time in UT)	Shock passage Date (time)	Ejecta (in situ) Date (time)	K_p Geomagnetic Index
1	12/2/96 16:40	04:00–18:00	? EP background	no	5–7 Dec 96?	2
2	12/19/96 17:40	15:56	no	no	24–25 Dec 96	2
3	1/6/97 17:34	14:30–16:30	1/8–11 RB (km TII)	1/10 00:52	10–11 Jan 97	6
4	2/7/97 02:30	02:07	2/7–11 EP (MeV)	2/9 12:55	10–11 Feb 97	5
5	4/7/97 14:27	14:00–14:10	4/7–13 EP	4/10 12:55?	10–11 Apr 97	7
6	4/16/97 07:35	14:13 day b.	no	no	21–23 Apr 97	5
7	4/27/97 10:26	02:18	no	5/1 12:00?	2 May 97?	6
8	4/27/97 14:59				(02:10–0600 UT)	
9	5/12/97 07:35	04:50–04:55	5/12–17 EP/RB	5/15 01:15	15–16 May 97	7
10	5/21/97 21:00	20:15–20:42	5/21–26 EP	5/26 09:16	26–28 May 97	6
11	7/30/97 04:45	20:00 day b.	no	no	3–4 Aug 97	5
12	8/30/97 01:30	23:32–23:41 day b.	9/3 01:00–9/4 14:00 RB	9/2 22:40	3–4 Sep 97	6
13	9/17/97 20:28	11:43–12:15 15:00–17:00	9/17–21 EP	9/21 04:10?	21–22 Sep 97	5
14	9/28/97 01:08	03:05	? EP background	10/1 00:57	1–3 Oct 97	7
15	10/5/97 15:02	08:50–10:15	10/7 05:20–12:30 RB	10/10 03:00?	10–11 Oct 97	6
16	10/6/97 15:23	~16:00		10/10 16:00		
17	10/21/97 18:03	17:34–17:54	10/21–25 EP	10/24 11:15	24 Oct (11:00–15:00 UT)	5
18	10/23/97 11:26	12:13–13:54	10/27 10:30–14:30 RB		27–28 Oct 97	4
19	11/3/97 11:44	09:10–10:31	11/4 06:00–11/5 04:30	11/6 22:10	6–8 Nov 97	7
20	11/4/97 08:27	05:57–06:13	RB, EP			

day b. = day before; ? EP background = uncertain EP-Event due to above background intensities, RB = radio burst, and ? = uncertain shock-ejecta association (under "Shock passage"); ? = uncertain identification (under "Ejecta. . .")

(IMC) of intense and ordered magnetic field, with a large flux-rope structure of approximately cylindrical shape and a cross section extent of more than one thousand Earth radii ($r_{\mathrm{FLUX-ROPE}} \sim 0.1$ AU; see, e.g. Klein and Burlaga, 1982; Lepping and Berdichevsky, 2000). IMCs are an important subset of ejecta (Burlaga et al., 1981; Marubashi, 1986) and are associated with the largest disturbances in the terrestrial magnetosphere (see reviews by Gosling, 1990, and Farrugia, et al., 1997a, and references therein).

Observations of conditions relating to ejecta in the solar wind are illustrated in Fig. 2. Starting from the top they are: in panel (a) a region of dominant magnetic energy, i.e. low β_p $(= (2kT_p)/(m_p V_A^2)$, where $T_p = m_p/2k\ V_{Th}^2$, with k the value of the Boltzmann constant, and V_{Th} the proton thermal speed, related to $\sigma = V_{Th}/\sqrt{2}$, the half-width of the plasma proton distribution and where $V_A = B/\sqrt{(4\pi N_p m_p)}$ is the Alvénic speed); unusually high $N\alpha/Np$ ratio in panel (b) (see, e.g. Zwickl et al., 1983); in panel (c) a comparison of T_p to the expected solar wind proton temperature (e.g. Lopez, 1987; Richardson and Cane, 1995); and in panel (d) unusually strong interplanetary magnetic field (Klein and Burlaga, 1982). Also shown in panels (e) and (f) are the latitude and longitude angles of the magnetic field showing its slow rotation, another ejecta signature used in our study. In addition, the solar wind velocity (not plotted in Fig. 2) is included in the analysis of the Sun-Earth connection event, because its value, in the ejecta interval, is useful to understand the event history and it also contains valuable information on the relationship between shock and the leading-edge of the ejecta. Notice that T_{expected} is the result from a well-established correlation between solar wind plasma proton distribution width and the speed of the solar wind (here we use T_{expected} by Lopez and Freeman, 1986, corrected for Wind by Richardson, private communication, 2000).

Low β_p (usually ≤ 0.1) results from the combined effect of strong magnetic field and low temperature T_p in ejecta. Zwickl et al. (1983) noticed the association with shock drivers of an unusual ratio of the alpha to proton density ($N\alpha/Np$) with respect to typical solar wind values (Hirshberg et al., 1972). In the low-speed solar wind, this $N\alpha/Np$ ratio is highly variable and lies in the range of 1.5–3.5%. In high-speed streams, this ratio is close to 4% (see Neugebauer, 1981 and references therein, and for WIND/SWE observations, see Steinberg et al., 1996). It must be kept in mind that ejecta at 1 AU are not associated with a unique set of signatures (Zwickl et al., 1983; Goldstein et al., 1998; Cane et al., 1998). Bidirectional electrons (Montgomery et al., 1974; Gosling, 1990) and cosmic-ray Forbush-decreases (see, e.g. Forbush, 1939; Cane et al., 1996) are two other trusted and commonly used ejecta signatures. These two observables are discussed in a comparison of our results with studies by other workers (see Sect. 5).

Table 2. Solar and low corona signatures

No. H-CME	CME ∠ Extension Date	V(CME) Leading Time	(S)OHO/EIT Signature Edge	S-EIT/GOES-SXT/ (Y)ohkoh-SXT/Hα Time	Location (EIT/SXT) Lon Lat (Type of Source) Other	SXR peak X-r flux	Metric (m) Radio Bursts Time	Deca-m Radio Bursts	SEP [1-20 MeV]
#/MDY	[°]/[UT]	kms^{-1}	[Sign]/[UT]		(+W/–E), (+N/–S)	[M]/[UT]	Type	Type/UT	onset/UT
1	360°	613	risng loops 0400–	SXR backgrd. > B1 f	77, −1.5? AR	C2.7?	?	no	Backg.
12/2/96	15:35		18:00	earlier big LDE		14:34‡			
2	300°	332	new arcade s.	Y loop erupt. 1556; DR;	19,−6↔0,−20 AR	C2.3 LDE	no†	no	no
12/19/96	16:30	∼15:56	sigmoid			15:56‡			
3	360°	211	not observing	Y loop dispp 1511	0, −28	A1 LDE?	no†	no	no
1/6/97	17:34			RAM: 1301–1453 FD		15:11			
4	360°	804	fil erupt onset	Y/EUV huge arcade;	49, −22↔−24,−35 lrge post	∼A5 LDE?	no†	III	∼2 MeV
2/7/97	02:30		02:07	LEA: 0107–0412 FD	erup arcade	04:00?		0230	1000
5	360°	826	EIT-wave	EUV DR, arcade;	−19, −30 AR.	C6.8 LDE	II, III, V	II, III	2–20 MeV
4/7/97	14:27		14:06 start	H0L: 1344–1355 FD		14:03‡	1356–1358	1400^{III}	15:45
6	145°	247	EIT-wave. 1451b	EUV ∼1436 start DR;	−4, −22 AR	∼C1 LDE?b	II	no	no
4/16/97	02:30			LEA: 0325–0330 FD		14:20/20:07‡	1416–1427b		
9	360°	260	EIT-wave	EUV DR, arcade; Hα:	6.5, 22 AR	C1.3 LDE	II	II, III	2–20 MeV
5/12/97	07:35		04:50 start	0443–0449 FD		04:55‡	0454–0503	$05:00^{III}$	07:30
10	≥170°	303	EIT-wave	EUV DR; SXR LDE;	12.5, 6 AR	M1.3 LDE	IV	II, III	2–20 MeV
5/21/97	∼21:00	after ∼20:00	mple Hα SF flares			20:15‡	2027–0023	20:50	22:00
11	360°	124	fil erupt onset	EUV fil erupt. continue	1,25↔1, 49	?	no (flare/FD	no	no
7/30/97	04:45		20:00b?	until ∼11:00?		backgrd >A3	at other loc)		
12	360°	427	EIT-wave	EUV DR; arcade	−15.5, 29 AR	M1.4 LDE	III	III	no
8/30/97	01:30		23:41b-start			23:32b‡	2331b	2345b	
13	360°	487	fil erupt onset	EIT-wave 1215 start; 3	−66,↔47, 20	M1.7 LDE	III, V	III	2/5 MeV
9/17/97	18:18–20:28		15:09	SXR LDEs	lrge post erup arcade	1143/1807‡	many	many	∼20/0230a
14	360°	355	fil erupt onset	rising loops >2230b DR;	−13,39↔20,14	B2 LDE?	III	no	Backg
9/28/97	01:50		∼2300b	EIT-wave 3UT		2237b	2237b		

b = day before; f = from; DR = dimming region, FD: disappearing filament (DSF), SXR LDE: soft X-ray long duration enhancement, AR: active region; ‡: optical flare; ↔ = approximated heliographic extension of a long filament before eruption. RAM, LEA, H0L = Solar Bulletin acronyms for heliospheric observatories.

A combination of sheath-ejecta indicated in Fig. 1 and presented in Fig. 2 are responsible for enhanced geomagnetic disturbances. For example, high dynamic pressure and southward IMF can be seen in panels (e) and (g) in Fig. 2. The large enhancements in K_p index (Panel (h) in Fig. 2) are a consequence of the disturbances caused by these solar wind conditions.

Twenty H-CMEs identified during the year, starting on 2 December 1996, are listed in Table 1. This list gives a time line for the possible stages of the Sun-Earth connection. In 18 cases, after some days, the planetary K_p index reached values between 5 and 7, which are well above the mean yearly average for 1997 ($\sim 1.6 \pm 0.9$, with median 1.5). For each event, Table 1 presents a sequence of times possibly relating to the H-CME observations on the Sun disk, inner heliosphere, and at 1 AU. Column 1 orders the events chronologically. Column 2 gives the date and time the H-CME was observed at 2 solar radii (R_s), followed in column 3 by the time(s) when we associate transient changes on the solar disk with the lift-off. Listed in column 4 are the time intervals of IP radio emissions and/or MeV EP. Column 5 gives the date and time of the shock passage at 1 AU. Column 6 shows the interval of observation of ejecta signatures at 1 AU by Wind, followed in the last column by the highest K_p value reached. As Table 1 shows, some events possess all stages of a Sun-Earth connection. A complete sequence of signatures occur in the case of Event 9, where Figs. 1 and 2 illustrate almost three days of manifestations at 1 AU of the shock driven by the ejecta in the inner heliosphere, the in situ observation of its passage on day four, followed by signatures of the ejected material (the 15 May 1997 IMC). The table further shows that there are cases where it is not possible to associate unambiguously a single H-CME with the corresponding near-Earth signatures. These are the cases when more than one H-CME appears to occur within short intervals. In the rest of the paper, we concentrate on the main features of the Sun-Earth connection for H-CMEs, separated in time by more than 4 or 5 days. This requirement leaves us with 12 H-CMEs. (See Appendices for specific, additional, observational facts, and their interpretation for Events 4, 5, and 9).

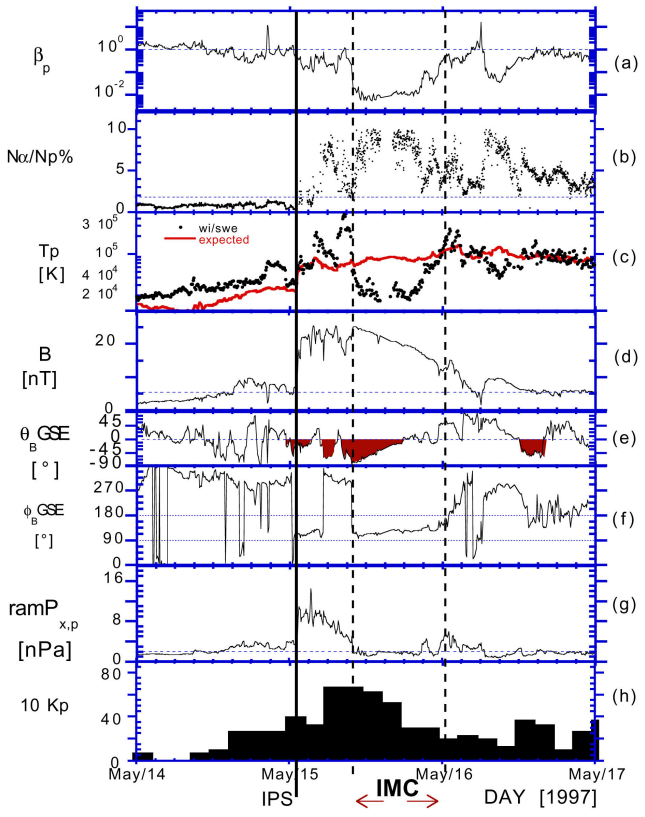

Fig. 2. Ejecta signatures used in this work (for Event 9) in panel: **(a)** proton plasma β_p; **(b)** solar wind He^{++} to H^+ ratio; **(c)** observed and expected proton temperature Tp; **(d)** intensity of the interplanetary magnetic field; **(e)** and **(f)** latitude and longitude orientation of the interplanetary magnetic field in GSE coordinates; **(g)** solar wind plasma ram pressure. Mid-latitude Earth's geomagnetic response index K_p is given in panel **(h)**. The dash-lines in panels (a), (b), (d), and (g) indicate the near ecliptic, approximate long-term solar wind mean values at 1 AU.

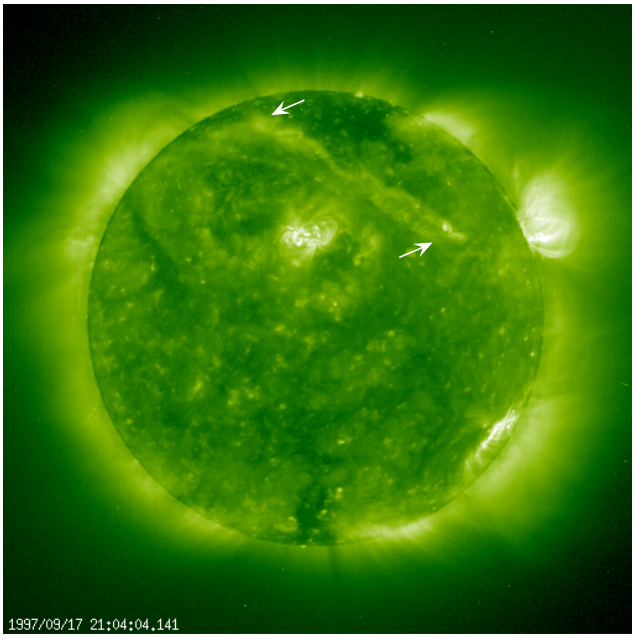

Fig. 3. White arrows show more than 60° extension of a new arcade formation after filament eruption (Event 13) in UVI 195 Å whole disk image of the low sun corona.

4 Statistical results

Table 2 presents the events for this statistical study. From left to right, in Table 2, the first column identifies the event number and date. The second column gives the angular extension of the H-CME and the time of observation of its leading edge's appearance in the LASCO C2 coronagraph (two solar radii occulting-disk). Column 3 gives the velocity in the plane of the sky of the leading edge of the CME. Column 4 gives the timing of the transient on the solar disk, in the low corona, using EUV images: EIT-wave start, filament eruption onset, rising loops or new arcade formation. Column 5 gives other SOHO/EIT signatures: dimming region (DR) and arcade formation after halo-CME (arcade a). When information was available, column 5 gives the time of a filament disappearance in Hα at approximately the same heliographic location as the EUV signature. Column 6 gives the location of the event on the disk relative to central meridian and the ecliptic plane. The possible relationship of the event with an active region (AR) is also indicated. The presence of a long duration enhancement in soft X-rays (1–8 Å) is indicated in column 7. This column also shows whether an optical Hα flare was observed at/near the lift-off location on the disk suggested by the coronal EUV and/or Hα chromospheric images. Column 8 gives the time and type of observed metric radio burst emissions and the onset times or interval duration of the metric Type II, III, IV and or V radio bursts. Column 9 features the observation of possibly related decametric radio bursts, Type II and/or III and their onset times. Finally, column 10 gives the onset time of 1–2 MeV energetic particles (long duration EP assumed to be associated to an ejecta driven shock).

In one case, for Event 3, SOHO/EIT data was not available and Yohkoh/SXT images show the disappearance of a hot loop, $\geq 10^6$ degrees Kelvin at 15:11 UT on 6 January 1997. Consistent with the location of the bright and hot loop disappearance, there is a report of a 11° long filament disappearance in Hα between 13:01 and 14:53 UT. The location is not cataloged as a sunspot or an AR. The EIT signatures of the observation, of rising loops and new arcade formation, are post eruption for Events 1 and 2. In Events 4, 11, 13, and 14 the EUV observations of the onset of the CME are the progression of filament eruptions starting two hours or more before the leading edge of the CME has been identified in the C2 coronagraph. For the Events 5, 9, and 12, the EIT-wave was observed within two hours of the CME. For Event 6, 16 April, a partial H-CME, the EIT-wave and more than one eruptive Hα flare occur several hours before the observation of this partial H-CME. A filament disappearance in Hα is reported about one hour after the time of this slow CME (Event 6) and several hours later, there are some

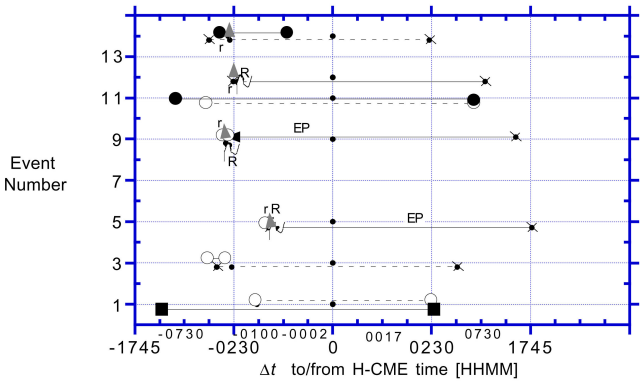

Fig. 4. Seven time lines of chromospheric and corona disturbances measured with respect to the observation time of the halo-CME (Table 2). The vertical axis indicates the event each time line belongs to. A solid line connects start and end times of a well identified solar disturbance, while a dash-line indicates a tentative identification. Open circle (o) stands for chromospheric filament disappearance; Solid circle (•) for filament eruption in UVI light; Crossed-dot (⋆) for soft X-ray LDE; Hatched-triangle (△) for optical flare; Solid-square (■) for new arcade formation; Curly-symbol for the onset of EIT-wave; letter "*r*" for metric radio bursts; letter "*R*" for the start of decametric radio bursts; Letters "EP" for the inferred start time of a gradual energetic particle event.

EUV signatures of a dimming region, all near the same heliographic location (4° E, 22° S).

4.1 EIT-wave versus EUV filament eruption

Table 2 shows the EUV EIT-wave occurrence for each AR related H-CME, when the cadence of the EIT/SOHO instrument allowed its observation. (Image examples are: for Event 5, panels 7 to 9 in Brueckner et al. (1998); for Event 9, Fig. 2 in Thompson et al. (1998); for Event 12, Plate IIa, this work). In these cases, the EIT-wave was observed before the H-CME. In each one of them, it was possible to identify a related eruptive Hα flare, metric radio burst activity, and a long duration enhancement (LDE) of soft X-ray solar radiation of several hours and peak intensity C1 or larger. We also encountered reports of Hα filament disappearance for each of these events, except in the case of Event 12. Therefore, an EIT-wave appears to be a clear EUV signature on the solar disk in the case of H-CMEs associated with filament eruption at an AR.

Table 2 also contains 5 EUV filament eruptions. (Image examples are Event 14 in Plate IIb, and a large post-eruption arcade formation in Event 13, Fig. 3). EUV filament eruptions appear to be associated with the expulsion of material from a filament channel that is also visible in Hα. However, only in 2 out of 5 of these cases is there a report of a filament disappearance in Hα within a few hours before the CME. Most of these cases do not show dimming after the EUV filament eruption. In some cases, after the eruption profuse, new arcades appear to form on top of the filament channel (e.g. right bottom inset in Plate IIb).

Seven representative time lines (Events 1, 3, 5, 9, 11, 12 and 14) are presented in Fig. 4 using a nonlinear time scale,$(\Delta t/1hr)^{1/3}$, with the difference Δt between solar transient and the leading edge observation of the H-CME (solid point at $\Delta t = 0$). In this figure, the start and end of the EUV observation of rising loops is indicated with solid squares, and with solid circles for the start and end of a filament eruption. The onset times of m-radio-bursts, decametric-radio-bursts, and flow of energetic particles are indicated with r, R and EP, respectively. Onset of EIT-wave activity is given by the curly symbol, a hatched triangle indicates the associated observation of an Hα optical flare, and crossed-solid-circle points to the start and end of a long duration enhancement of the 1–8 Å wave length soft X-ray. Finally, white circles give the times of observation of a filament disappearance in Hα.

Figure 4 shows AR related Events 5, 9 and 12, from Table 2. Here, we find that the lift-off of the AR related solar transient showed the following in close succession: 1st filament in Hα disappears (but no record for Event 12); 2nd, onset of metric radio burst emissions a few minutes later (may be missing in Event 12 due to a continuum radio burst storm at the Sun); 3rd, an eruptive optical Hα flare starts or its peak emission is reached (from the Solar Bulletin). After that, 4th, onset of decametric radio burst (80% of the cases) and EIT-wave follow. Following these steps, the H-CME is observed. The start time of the eruptive Hα flare coincided with the onset and/or peak emission of a 1–8 Å soft X-ray LDE event with above background emissions lasting for several hours (peak output indicated by a solid dot on line connecting crossed solid points in Fig. 4). After the H-CME, there are one or two long lasting dimming regions and continuous arcade formation, or rising loop activity.

A time line relating EUV filament eruption with the later observation of an H-CME does not show any other consistent solar disk signature (this is illustrated by the time line for Events 11, and 14 in Fig. 4). In Event 11, no enhancement in 1–8 Å soft X-ray appear to exist, and this is questionable in Event 14, where the possible enhancement is indicated with a dashed instead of a solid line, connecting crossed-solid-points in Fig. 4. An EUV filament eruption appears for events with a previously Hα quiescent filament-channel as the only apparent source of a CME which seems to be unrelated to any AR; this may also be the case for Event 3 in Fig. 4. (For Event 3, Yohkoh SXT images show the disappearance of a hot coronal-loop; Webb et al., 1998). The long duration rising loop observation in Event 1 (Table 2 and Fig. 4) is less clear, belonging to an event near the west solar-disk limb. (Here, it must be noted that besides the discussed observations of the corona in EUV light, coverage is complete for decametric radio emissions and MeV EP, but for metric solar radio emissions and Hα observation of the Sun's chromosphere, we rely on information in the *Solar Bulletin* and private communications). In the case of the large filament eruption in Event 13 (Table 2), there are time coincidences with an EIT-wave, Hα optical flare, 1–8 Å soft X-ray LDE, metric and decametric radio bursts, and the onset of the long

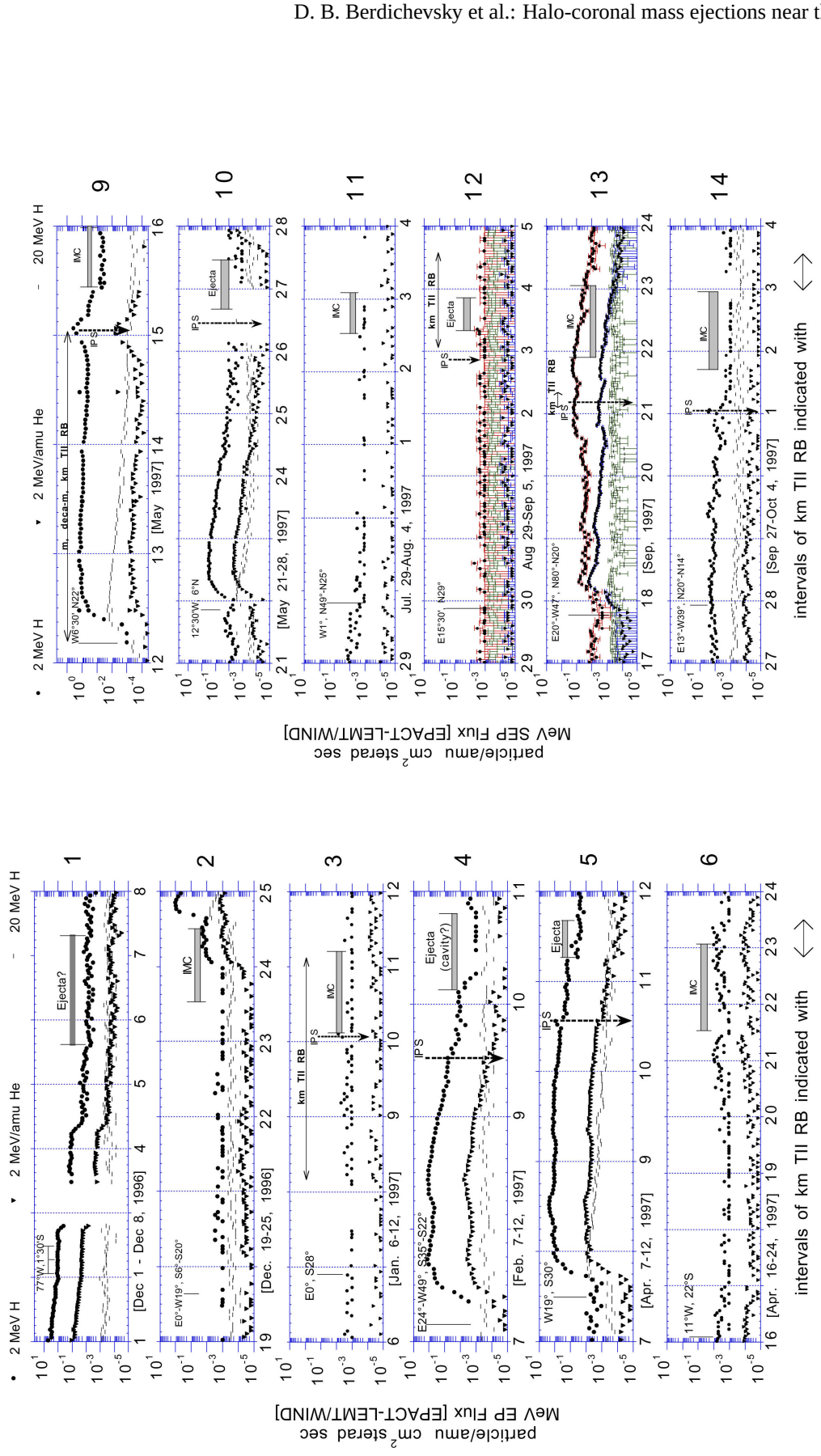

Fig. 5. For each event a panel shows 2 MeV/amu H^+ and $^4He^{++}$ EP fluxes, and 20 MeV H^+ fluxes. EP for each event is presented from the start of the Sun-Earth connection to the local observation of the ejecta material. The event number is shown to the right of each panel. In each panel, the following are indicated: the vertical line/bracket (on the left) gives the start time of the Sun-Earth connection event. We also indicate the likely location on the solar disk of the corresponding transient source. The ejecta time interval on the right is marked with a thick bar-like shaded area. A horizontal line ending and starting with arrow heads indicates the time interval of kilometric Type II radio bursts, when observed, and a vertical thick dash arrow marks the in situ observation of the interplanetary (IP) shock. (Error bars show background levels and statistical errors in panels 4th, and 5th from the top, in Fig. 5b.)

duration energetic particle event. In this case, it is not possible to separate the radio and EP signatures from a possible association either with this H-CME or other CMEs at the solar-disk limb.

4.2 Inner heliosphere signatures

Metric Type II radio emissions are interpreted as the signatures of a shock moving away from the Sun from the very base of the Sun's corona. These radio emissions are related to local corona density encountered by the shock (see, e.g. Cane and Stone, 1984). Table 2 shows Type II and other types of metric and decametric radio emissions. The density is lower and decametric radio emissions are expected when the shock reaches approximately 2 to 12 solar radii. Radio emissions other than Type II radio bursts can be "shock associated" signatures. They are metric "herring-bone" radio bursts, complex metric and/or decametric Type III radio bursts, and also Type IV and V radio emissions (see, e.g. Cane et al., 1981; Bougeret et al., 1998). In four out of the seven AR related CMEs, there were observations of decametric radio burst emissions. In three of these cases, the onset of the long duration MeV EP event was observed. In two out of five of the CMEs unrelated to AR, there was observation of decametric radio burst emissions and the onset of MeV EP long duration enhancements. These radio emissions and EP observations are consistent with a possible interplanetary shock, which may be driven by the CME as it moves outward in the inner heliosphere (see, e.g. Sanahuja et al., 1983; Cane et al., 1986). The earlier arrival of the more energetic protons accelerated by the shock close to the Sun allowed us to identify the beginning of the event in the MeV EP (see e.g. Cane et al., 1988; Reames et al., 1996). Table 2 shows that at least 5 events have the MeV EP signatures, suggestive of the presence of a shock close to the Sun. These are Events 5, 9, 10, 12, and 13 (i.e. 7–11 April, 12–15 May, 21–27 May, 29 August–5 September, 17–23 September 1997). For Event 4 (7–11 February 1997), Table 2 lists a rise in shock EP several hours later ($\sim$ 10 UT, 7 February).

Figure 5 shows the intensities of 2 MeV protons, 8 MeV He^{++} ions, and the 20 MeV proton channels from the start until the passage at 1 AU of the candidate ejecta interval, for every event. The vertical line on the left of each panel gives the event start time, and the possible heliographic location on the Sun of the observed main feature(s) associated with lift-off. Arrowed horizontal lines indicate the interval of observation of drifting radio emissions. The pointing down, thick-dashed arrow on the right, gives the time of the in situ observation of the IP shock. The shaded thick horizontal bar-like symbol on the right side in each panel indicates times of passage by the Earth of the candidate ejecta.

Figure 5 shows that in some cases shock signatures in the inner heliosphere are the enhancement of MeV EP, in others kilometric Type II radio bursts, and in a few cases, both indicators were observed. One or both indicators are present for Events 3, 4, 5, 9, 10, and 13 (see corresponding panels in Fig. 5). A combined check of Table 2 and Fig. 5 for Event 3 shows no signatures of shock near the Sun, but clear signatures of a shock in the inner heliosphere. (Intense kilometric Type II radio bursts, i.e. radio emission enhancements, start at a wavelength corresponding in this case to about 0.5 AU; Reiner et al., 1998a).

The decrease in the flux of MeV EP during the candidate ejecta intervals, consistent with shielding, by closed or partially closed magnetic field lines, is observed in the case of Events 1, 4, 5, 6, and 9. Inconclusive is the case in Event 10 due to a data void, and hindrance of MeV EP during new injection while the ejecta passage by the Earth is possible in Event 2.

A closer look at Fig. 5 shows that the IP background for 2 MeV protons lies at or near a flux intensity of 10^{-3} particle/(cm^2 str s), while for 8 MeV He^{++} ions and 20 MeV protons it lies at or near $10^{-4} - 10^{-5}$ particle/(cm^2 str s). The MeV EP velocity dispersion at the start of the isolated Events 4, 5, 9, and 10 identifies them in Fig. 5 as the events for which MeV EP enhancements provide indication of a shock propagating from the Sun outward into the inner heliosphere. Incomplete indication of a shock propagating in the inner heliosphere with MeV EPs is the result of high background possibly due to an earlier or later limb event. (Notice that from Table 1 we keep intervals when H-CMEs do not overlap in time, but other long lasting gradual EP events do contaminate some of the intervals of interest). In the case of Event 13, the presence of a new injection around 09:00 UT on 20 September obscures the later relationship of these MeV EP to the approaching shock, which was observed near Earth at 04:10 UT on 21 September. MeV EP background from earlier event(s) was present for Events 1 and 14. No MeV EPs were observed for the other four events. Shock spikes beginning ahead of the IP shock were observed for Events 4, 5, 9, and 14. In these cases, the spike-like MeV EP flux enhancements add at least two hours of warning that a shock is approaching Earth.

The tracking or sensing of the shock location from afar through its Type II radio bursts, i.e. radio emissions at the interface with the upstream solar wind, is also indicated in Fig. 5. In addition to the full Type II radio bursts tracking in Event 9 (see also top panel in Fig. 2), we can also identify three partial trackings (Events 3, 13, and 14). For Event 13, 17–24 September 1997, the corresponding panel in Fig. 5 shows that Type II radio bursts were observed from around two hours before the IP shock up to four hours after, which would suggest a lateral encounter with the shock region generating the Type II radio bursts. Kilometric Type II radio bursts in the 6–11 January and 29 August–5 September 1997 events are long-duration kilometric Type II radio bursts, which ended many hours after the passage of the IP shock. In the second case, Event 12, they were actually observed only downstream of the shock. These two events lacked the presence of MeV EP fluxes. These cases of drifting radio emissions, ending behind the IP shock, may have originated at a shock location hundreds of Earth radii away from the local in situ observations.

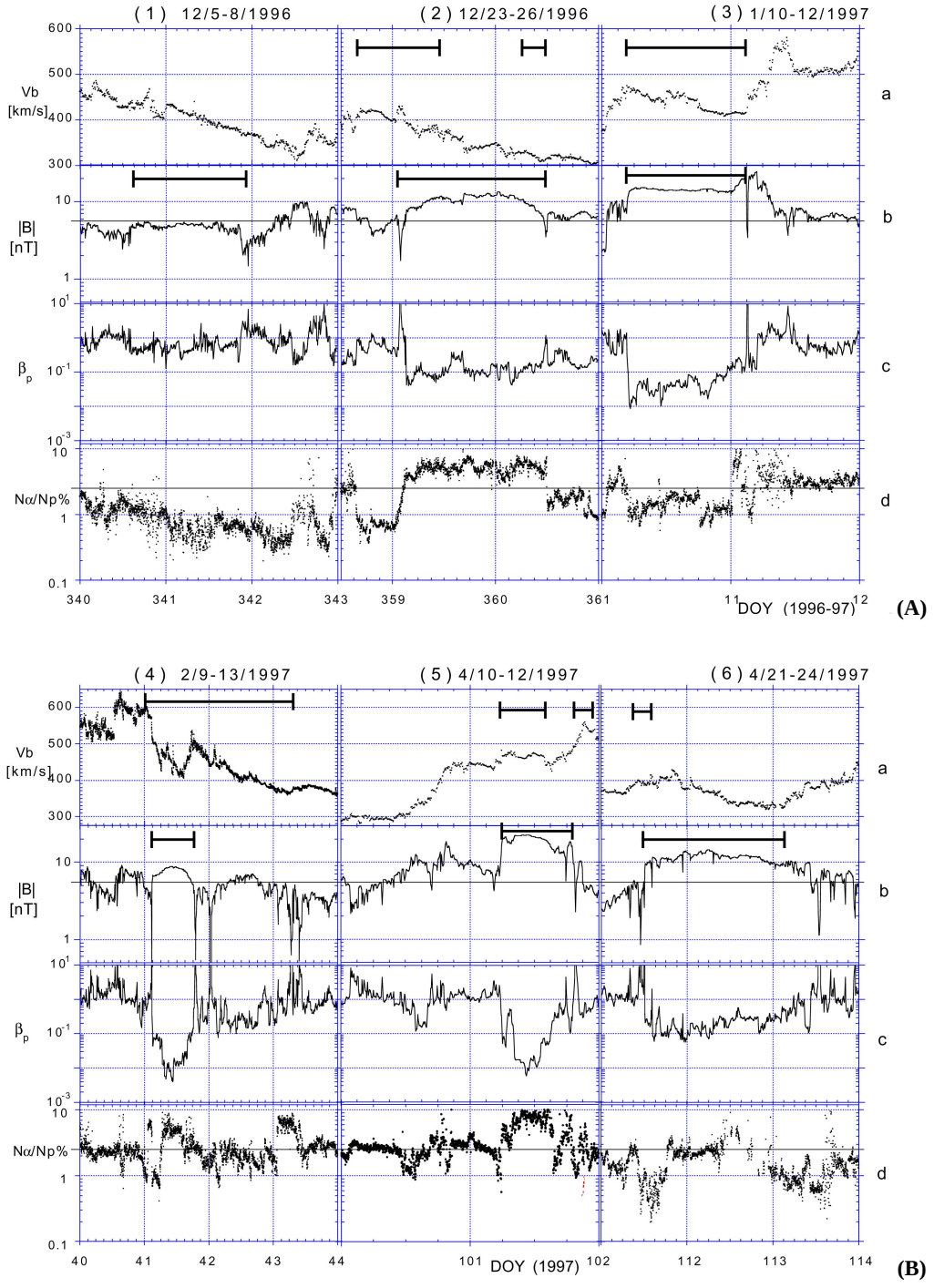

Fig. 6. Candidate ejecta intervals, at 1 AU, are ordered chronologically from left to right. On top of each panel-column, for each event, its order-number and interval of solar wind observation is given. Panel **(a)** shows solar wind velocity and horizontal bar indicates times when $Tp < 0.5T_{\text{expected}}$; Panel **(b)** shows magnitude of the interplanetary magnetic field, horizontal bar indicates largest time interval of a slow rotation of its orientation, and horizontal line indicates historical mean value of 5.5 nT. Panel **(c)** shows the β_p plasma parameter; Panel **(d)** show the percentage alpha to proton relative abundance $N\alpha/Np\%$, the historical average value ($\sim 2.3\%$ for a slow solar wind) is indicated by the horizontal line.

4.3 In situ observations at 1 AU

Identification of the ejecta interval is not free of ambiguity (for a recent statistical investigation, see, e.g. Goldstein et al., 1998). Notice that Table 1 in its three right columns, from left to right, gives the time of the passage of the interplanetary shock by Wind, the day(s) of unusual and/or disturbed solar wind conditions in the Earth's vicinity and the maxi-

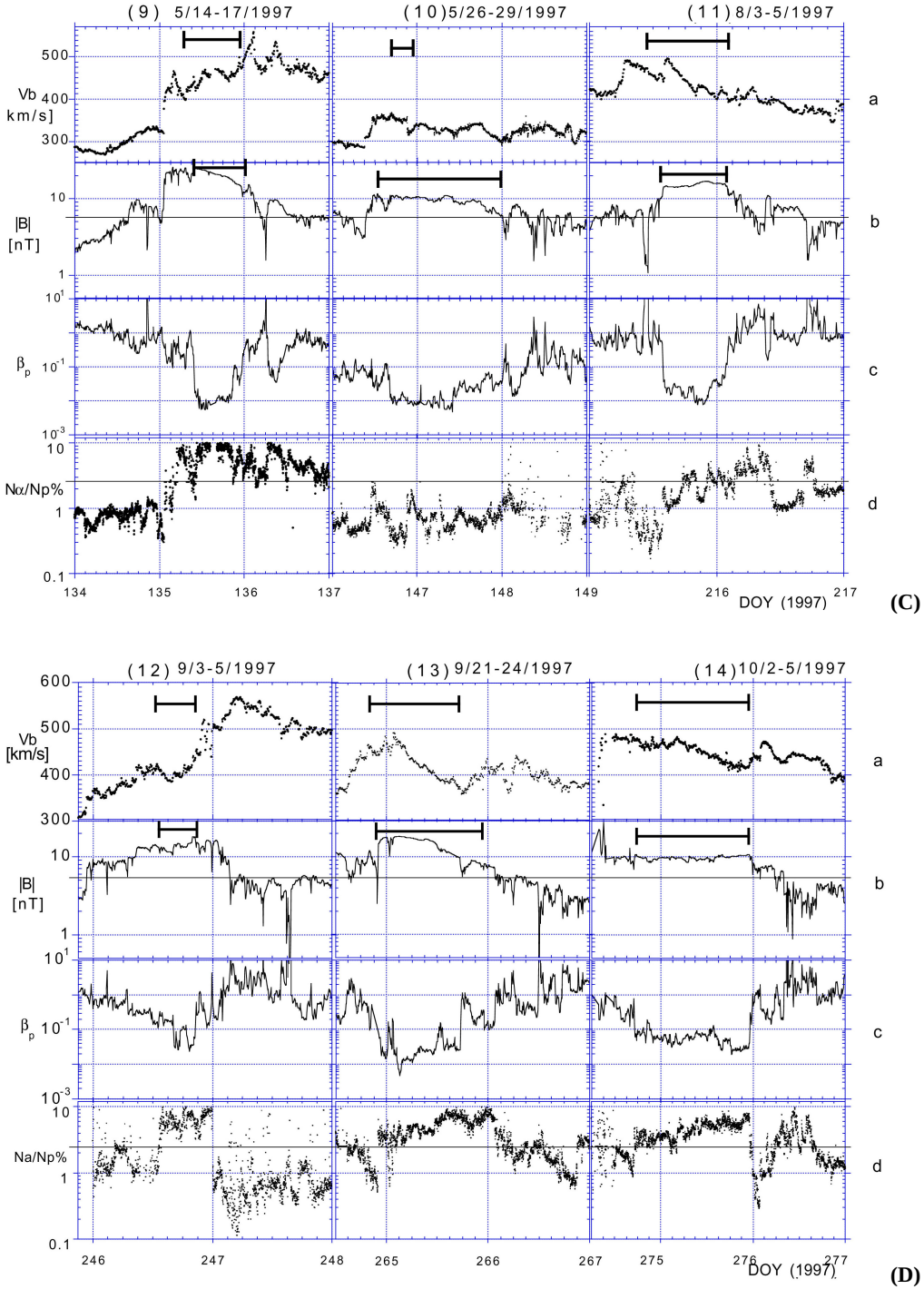

Fig. 6. ibid.

mum observed geomagnetic K_p index value. In our search of the ejecta candidate time-interval(s) in Events 3, 4, 5, 9, 10, 12, 13, and 14, we focus on solar wind conditions downstream to the passage of the possibly driven interplanetary shock. In the other four Events 1, 2, 6, and 11, no shock is observed; however, in all cases we search for similar identifying signatures. In Figs. 6A–D, we ordered by column the plots for each event. At the top of each plot-column we enter the event number and date, while below we place two to four day plots of a sample of solar wind parameters used for the identification of the corresponding ejecta interval. For each event, the top panel in Figs. 6 contains the plotted solar wind speed (panel a). In this panel, bar(s) indicate(s) interval(s) of a proton temperature (Tp) less than 50% of the one expected. The second panel from the top presents the magnitude of magnetic field (panel b). In this panel, the horizontal bar in-

Table 3. Ejecta signature intervals at 1 AU to the nearest hour

No.	Large, Slow Rot. of the $\boldsymbol{B}$ field	$\boldsymbol{B}$ field $\geq$ 1.5 aver.	$T_p/T_{\text{expected}} \leq 0.5$	Low β_p regions	$N\alpha/Np \geq 6\%$	Ejecta Region
Event	Time interval	Time interval	Time interval	Time interval	Time interval	Time interval
1	15 12/5–23 12/6	no	no	none♦	none (†)	?
2	02 12/24–12 12/25*	02 12/24–12 12/25	16 12/23–11 12/24 06-12 12/25	03 12/24–12 12/25	06 12/24–12 12/25	16 12/23–12 12/25
3	05 1/10–03 1/11*	05 1/10–09 1/11	05 1/10–03 1/11	05 1/10–03 1/11	00–8 1/11	05 1/10–07 1/11
4	03–19 2/10⇐	03–21 2/10	00 2/10–11 2/12	03–19 2/10	01–04, 07–10 2/10 02–18 2/11	00 2/10–11 2/12
5	06–19 4/11⇐	06–19 4/11	06–15 & 20–23 4/11	06–15 4/11	06–19 & 20–22 4/11	06–19 4/11
6	12 4/21–03 4/23*	12 4/21–11 4/23	09–15 4/21	16 4/21–03 4/23	minor enhancement	12 4/21–03 4/23
9	09–24 5/15*	05–24 5/15 06-14 5/16	07–24 5/15	10–24 5/15 06–14 5/16	05 5/15–03 5/16 06–13 5/16	05 5/15–13 5/16
10	12 5/26–00 5/28	09 5/26–00 5/28	17–23 5/26	16 5/26–10 5/27	none (†)	12 5/26–00 5/28
11	14 8/3–03 8/4*	13 8/3–03 8/4	10 8/3–03 8/4	14 8/3–02 8/4	04–11 8/4	10 8/3–03? 8/4
12	13–23 9/3	07 9/3–00 9/4	12–23 9/3	08–21 9/3	14–24 9/3	13-23 9/3
13	22 9/21–18 9/22*	22 9/21–18 9/22	20 9/21–18 9/22	22 9/21–02 9/23	11 9/22–02 9/23	22 9/21–18 9/22
14	16 10/1–23 10/2*	18 10/1–23 10/2	18 10/1–23 10/2	17 10/1–23 10/2	05–23 10/2 07–15 10/3	16 10/1–23? 10/2

(♦) During most of this interval 5-min average β_p are close to 1. Interval shows, from 10:00 UT 6 Dec to 07:00 UT 7 Dec, unusual anti-correlation between proton thermal-velocity and density
(⇐) Event described as cloud-like because the selected time interval has the features of an IMC, except for a narrower rotation of the IMF
(*) Event includes overlaps with interval identified as an IMC (Lepping et al., 1999).
(†) In Events 1, and 10 there are uninterrupted unusually low $N\alpha/Np$ (< 1%) from 00:00 UT 5 Dec to 12:00 UT 7 Dec 1996 and from 00:00 UT 27 May to 00:00 UT 28 May 1997, respectively.

dicates the longest time interval of a slow rotation of a 5-min average magnetic field. The third panel from the top presents proton plasma beta (panel c), β_p, and the bottom panel is the ratio of alpha to proton densities, $N\alpha/Np\%$ (panel d). A solid line across the $|B|$ panel indicates the approximate historical value of 5.5 nT (see, e.g. Burlaga, 1995), and in the case of the $N\alpha/Np\%$ gives 2.3%, which is in the approximate mean range of the values observed during intervals of slow solar wind (see, e.g. Neugebauer, 1981).

For the times plotted in Figs. 6, we search for candidate ejecta intervals with a duration of eight or more hours between sharp discontinuities in the value of B and solar wind speed, V. Ejecta indicators used are the slow rotation of the magnetic field $\boldsymbol{B}$, above average $|\boldsymbol{B}|$, low Tp, low β_p, unusual $N\alpha/Np\%$. The identified time intervals are listed in Table 3.

A closer look at Figs. 6B and C shows that in Events 4 and 9, high $N\alpha/Np\%$ appears in closer proximity to the driven interplanetary shock than the low β_p regions. Figures 6A–D show further that regions defined by high $N\alpha/Np\%$ and low β_p overlap with each other in Events 2, 5, 9, and 12. Additionally, high $N\alpha/Np\%$ regions are found in the rear part of the low β_p intervals for Events 3, 13, and 14, and are also found trailing the low β_p intervals of most events (Events 3, 4, 5, 9, 11, 12, 13, and 14).

The listing in Table 3 of overlapping time intervals for the diverse set of signatures shows support for the observation of ejecta in all cases except Event 1. Particular to Event 1 is the orientation of the interplanetary magnetic field during the middle of its smooth rotation, which for many hours it stays close to the Sun-Earth direction (during this whole interval Wind/SWE, after perigee, intermittently detects bow-shock upstreaming electrons; Fitzenreiter, private communication, 2001). Here, the main supporting signatures are the overlap of this slow rotating magnetic field with unusually low $N\alpha/Np\%$.

Adding the times of the overlapping and non-overlapping regions: (a) of large and slow rotation of the $\boldsymbol{B}$-field; (b) large $|\boldsymbol{B}|$ ($\geq$ 1.5 historical mean B); (c) low Tp; (d) low β_p intervals and (e) unusual $N\alpha/Np\%$ values, in Table 3, probably gives an upper limit to the possible elongation in time of the ejecta. These are our choices in the right column in Table 3, with the constraint that there is at least some overlap between two intervals, or the ejecta candidate intervals are closer than two hours to each other. We conclude that common to every interval is an extended region of a slowly

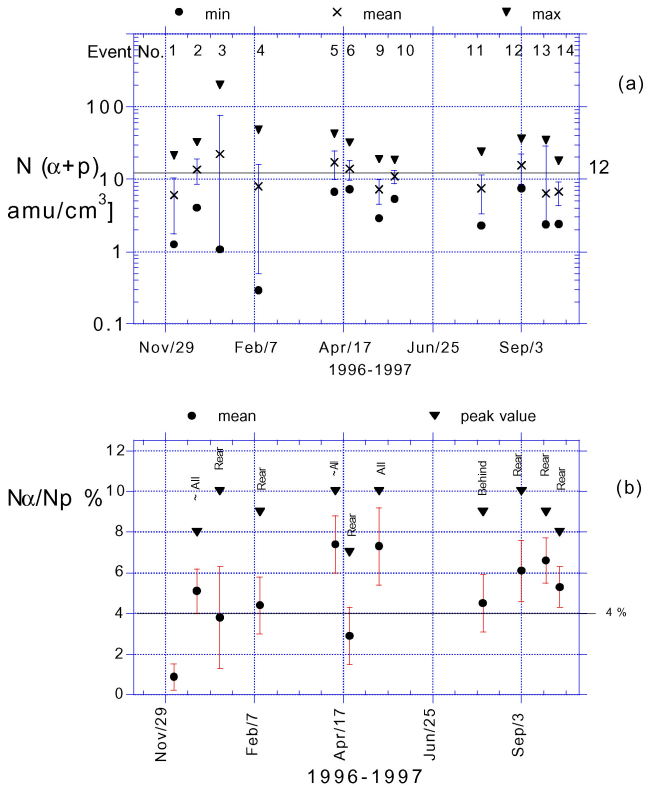

Fig. 7. Panel **(a)** shows for each ejecta the total plasma density [N(H^+) + N($^4He^{++}$)] maximum value (inverted full-triangle), mean and its mean fluctuation (cross with error bar) and the minimum value (full-circle). Panel **(b)** shows for each event the relative alpha to proton ratio $N\alpha/Np\%$ maximum enhancement (inverted full-triangles), mean and the 1 standard deviation (s.d.) ($N\alpha/Np\%$) of its mean fluctuation (full-circle with error bar). In the top side of Panel (b) the location in/near the ejecta of the $N\alpha/Np\%$ enhancement(s) is indicated.

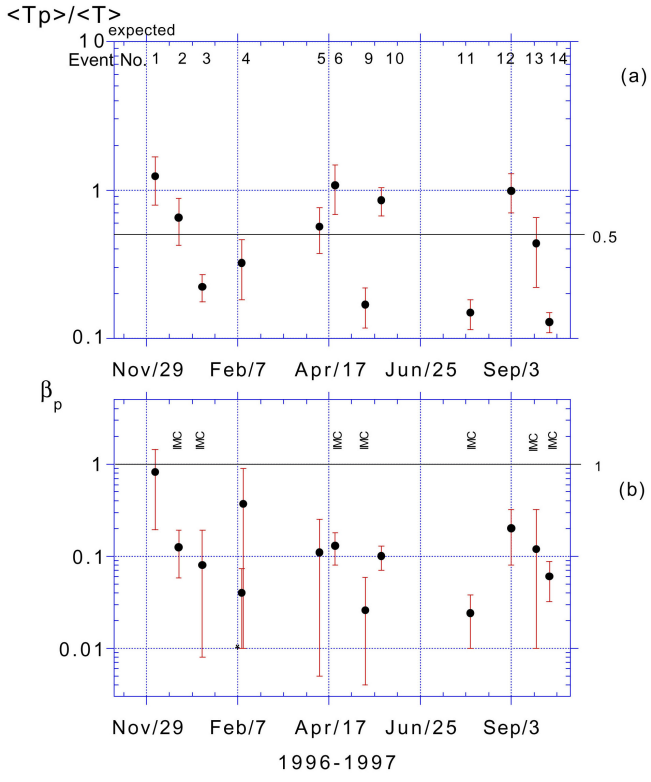

Fig. 8. In Panel **(a)** full-circles show for each event the ratio of the observed mean to expected proton temperature ($\langle Tp\rangle/T_{\rm expected}$). In Panel **(b)** full-circles show the mean β_p for each event. Panel (b) also indicates, with the acronym IMC on top, the ejecta that strongly overlaps with a time interval identified as an interplanetary cloud, fitted using the Lundquist force-free flux-rope model.

rotating magnetic field with partial overlap with one or more regions of unusual $N\alpha/Np\%$. Other observable indications of the possible presence of ejecta in the solar wind are discussed for these intervals in Sect. 5, in the context of analyses by other workers. Under this criterion, Wind encounters an ejecta interval in each event. When low Tp, slow magnetic field rotation, above average $\boldsymbol{B}$-field intensity, low β_p, and unusual $N\alpha/Np\%$ time intervals overlap, we obtain an alternative criterion for ejecta. The shortest extension would result from this alternative criterion of ejecta. In this way we also would be left with fewer ejecta encounters, and this is the case because an all-regions-overlap may occur between a few hours and a more extended duration for Events 2, 3, 4, 5, 9, 12, 13, and 14. At the same time, we can have a higher degree of confidence that these eight solar wind intervals contain an ejecta region. Still, ejecta at 1 AU are understood as plasma embedded in magnetic field domain still connected to the Sun, or to itself, with a volume equivalent to a scale length of several thousands of Earth radii. Hence, a volume of this size would show some shielding to EP, in general, and cosmic rays in particular. The changes in the intensity and/or anisotropy in the flux of EP and Forbush decreases are discussed in Sect. 5, in the context of the results presented by other workers.

For the listed ejecta time intervals (right column in Table 3), Figs. 7 to 9 present mean, minimum and maximum values for several solar wind parameters. Mean ($Np + N\alpha$) values, for these time intervals are close to 12 atomic mass units (amu) per cubic centimeter (see Fig. 7a). Extreme variations in plasma densities occur for most intervals. Only Events 5, 6, 9 and 10 show plasma density variations of less than one order of magnitude. The remaining intervals show an increase of one to more than two orders of magnitude from minimum to maximum plasma density. Similarly strong variations are present in the plasma composition ratio $N\alpha/Np\%$, as indicated by the mean and maxima values in Fig. 7b. Maxima values are 10% in Events 3, 5, 9, and 12, and 8–9% in Events 2, 4, 13, and 14. Unusually low $N\alpha/Np\%$ values exist in Event 1 and in most of Event 10. Above average $N\alpha/Np\%$ values trail the ejecta intervals in Events 5 and 12. Figure 8a shows that the mean $Tp/T_{\rm expected}$ ratio was 0.5

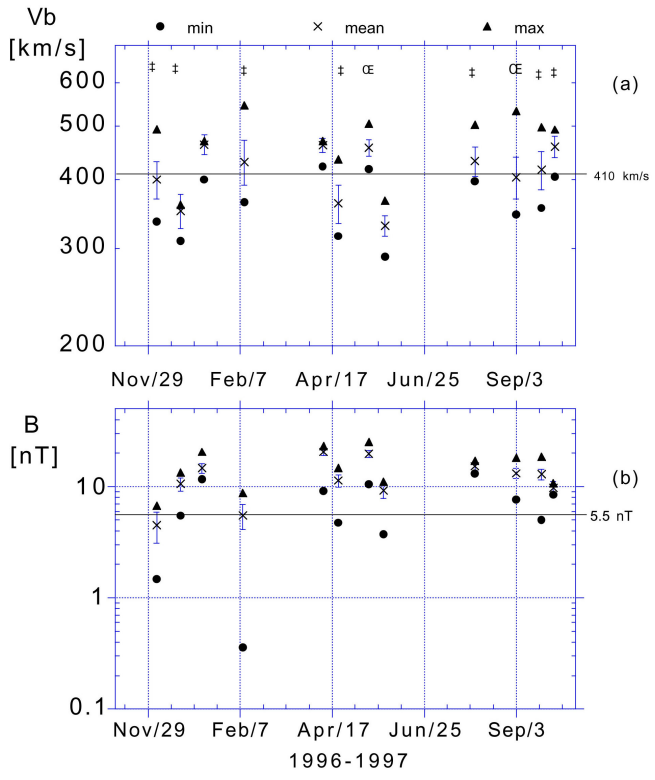

Fig. 9. For each event, panels **(a)** and **(b)** present magnitude values of solar wind speed V and magnetic field $\boldsymbol{B}$ of the ejecta. Maximum values (full-triangle), mean values, and the 1 s.d. deviation of its mean during the passage of the ejecta (cross with error bar), and minimum values (full-circle) are given for each event. In top of panel (a), symbol ‡ (Œ) indicates ejecta with a solar wind velocity showing a negative (positive) gradient as a function of time, while no symbol was given for cases showing a flat velocity profile as a function of time. In each panel, horizontal line with value on the right gives the corresponding historical solar wind value of the observable.

or less in Events 2, 3, 4, 5, 9, and 11. A mean value close to 1 is given for Events 1, 6, 10 and 12. For these cases, $Tp/T_{\rm expected}$ is less than 0.5 near the front of Events 6 and 10, and in the rear of Event 12, while absent in Event 1. Figure 8b gives the corresponding value of $\langle\beta_p\rangle \pm \sigma(\beta_p)$. All intervals, except for Event 1, show $\langle\beta_p\rangle$ values close to 0.1 or below. Two values of $\langle\beta_p\rangle$ are given for 9–12 February 1997 ejecta, with the lower value corresponding to the "cavity" region indicated in the Appendix. Figure 9a presents the $\langle V\rangle \pm \sigma(V)$, minima and maxima, respectively. In six ejecta, the bulk speed profile had a front-to-back negative gradient consistent with radial expansion, indicated with (‡) in Fig. 9a. Two cases in Fig. 9a, indicated with (Œ), had a much less common positive slope in V, suggestive of a possible interaction with a faster solar wind stream (see Farrugia, 1997b). In most cases, the depleted density region in the ejecta showed a sudden drop in the value of V, a correlation whose cause is at present unclear ($Vmin \ll V - \sigma_V$). This effect can be seen to stand out particularly in those cases of ejecta having a flat profile in V, and it can be seen from a comparison of Figs. 6 and Fig. 9a. Figure 9b shows that the average magnetic fields of the ejecta are well above the overall interplanetary value of $\sim$5.5 nT in 10 of 12 cases, with maxima being $>$ 20 nT in Events 3, 5, and 9. Two very low values ($|\boldsymbol{B}|$ min) result from interplanetary magnetic holes. The intervals of a smooth rotation of the $\boldsymbol{B}$-field, listed in Table 3, change orientation from north to south in Events 1 and 2. Conversely they change direction from south to north in Events 3, 6, 9, 11, and 12. They stay south in Events 4 and 10 and north in Events 5, 13, and 14.

5 Discussion

In the discussion, we attempt to present a statistical analysis of our observations. In this regard, we benefit from the complementary as well as partially overlapping work by other authors. Primarily, we notice that from a set of CMEs observed with the SOHO/LASCO instrument from January 1996 to June 1998 (St. Cyr et al., 2000), a H-CME has been added (not included in our list, Table 1). Webb et al. (2000b) include this event and indicate that it is seen at two solar radii at $\sim$07:00 UT on 9 March 1997 with a measured leading edge speed of approximately 150 km^{-1} in the plane of the sky. Webb et al. (2000b) also indicate that for this extra event there is no record of optical Hα flare, and the enhancement in 1–8 Å soft X-rays peaked at the level of a B3 flare. There is an observation of EUV dimming region at or near N 3 E 75. Approximately 69 hours later, a convected three-hour high density structure ($Np \sim 40\,\mathrm{cm}^{-3}$) travelling at 350 km^{-1}, too slow to be related, is followed by a possibly corotating interactive region. There is neither observation of a related shock, nor other indication of ejecta in the solar wind conditions between 3 and 6 days after this H-CME, and we agree with this interpretation. Statistical considerations presented below include this additional isolated H-CME, raising the number to 13 (21 when added to Table 1).

As in a detailed case study in Thompson et al. (1998), we find that it is possible to identify the solar disk source region with the heliographic start location of an EIT-wave in cases when the H-CME appear associated with an AR. EIT-waves seem to coincide in time with decametric Type II radio bursts, as indicated in the Appendix. (For a more detailed account, see Reiner et al., 1998a; Berdichevsky et al., 1998). For these AR related H-CMEs a chronological evolution is apparent with time line durations of 150 min or less (see time sequences in Table 2 and Fig. 4). This is consistent with Δt time intervals usually considered (see, e.g. Webb et al., 2000b; Hudson et al., 1998). In the case of quiescent filament eruption, or related to a decayed AR, Table 2 and Fig. 4 time lines show time differences between solar disk signatures and H-CME observations 4 to 6 times longer than the ones usually considered. A comparison of these two types of filament eruption, in Sect. 4.1, suggests two possibly different ejecta lift-off mechanisms. In one case, a filament in/near an AR needs to break layers of strong magnetic flux regions

in the process of lifting off. This requires large amounts of stored energy which are released faster, causing major detectable amounts of dissipation at the source region and almost always, these solar transient events have been identified in connection to double ribbon optical Hα flare, coinciding with an appreciable enhancement in the emission of soft X-rays. In the other type of lift-off – represented by five examples of filament eruption in EUV light – a scenario is suggested in which filament-like material, already above the chromospheric region, breaks loose at a relatively slow speed. In this type of lift-off, a favorable location for moving along a neutral line (source of the heliospheric current sheet) is required. This is suggested in the case of the nearly steady outflow of the solar wind during the last solar minimum (see, e.g. Michels, 1998). Here, low detectable dissipation would occur because less stored energy release is needed. Weak double ribbon flares may also be associated with their lift-offs and an identification has been made for Event 14 (Martin, private communication, 2001). After its lift-off, the ejected material becomes an H-CME when moving along the line of sight. These ejecta may be moving at slower speeds than the ones discussed in Cane et al. (1986), where all of them produce shocks which accelerated MeV EP.

Regarding the heliospheric latitudinal source of the H-CME, Table 2 shows locations that deviate in some cases strongly from the Sun's equatorial plane. This is consistent with the mean source locations at $\pm 30^\circ$ with respect to the Sun's equator of more than 100 CMEs, including H-CMEs, between April and December 1997. Beyond two solar radii propagated in mean value approximately in the ecliptic plane (Plunkett et al., 2001). In a case study, for Event 9, Webb et al. (2000a) presented this complex, non-radial propagation at the beginning of the ejection. The compiled set of EUV observations of EIT-wave and filament eruption identify as source regions of the H-CMEs the same or nearly the same solar disk locations in comparison to those identified for corresponding events in Webb et al. (2000b), and Hudson et al. (1998). (Webb et al. and Hudson et al. use for the identification of the time and location of the source STX/Yohkoh images, Hα dark filament disappearance, metric radio burst times, and two ribbon optical Hα flare, and like us, infer the possible association of 1–8 Å X-ray LDE).

Several H-CMEs presented drive a shock. For an overlapping subset of events, these shocks are also identified in Webb et al. (2000b) and Cane et al. (1998). In Sect. 4.2, we identify the cases where the presence of the driver (the ejecta) may be inferred in the inner heliosphere by the observation of shock-signatures in decametric and/or kilometric Type II radio bursts and MeV shock energized particles. They are present for individual cases in Hoang et al. (1998), Reiner et al. (1998a,b), Kaiser et al. (1998), Berdichevsky et al. (1998), Gopalswamy et al. (1998), and Webb et al. (2000a). For Events 3, 4, 5, and 9, Torsti et al. (1998) also present a study of EP and their interpretation of an ejecta-driven shock accelerating a seeded population of particles. Their analysis is based on observations with the SOHO/ERNE instrument. For Event 5, Torsti et al. (1998) call attention to the presence of a prompt EP Event ($\sim$ 30–50 MeV H) at the Sun and interpret it as "caused by a DC electric field acceleration during magnetic reconnection triggered by the solar eruption". The tracking obtained and/or inference of the shock in the inner heliosphere supports the association of the ejecta encountered later with the driver and makes a case for the validity of the Sun-Earth connection for Events 3, 4, 9, 10 and 13.

The proximity of a subset of these H-CME to coronal magnetic holes extending equatorward was pointed out in a study of the solar minimum sources of geomagnetic activity between October 1996 and July 1997 by Watari and Watanabe (1998). In agreement with their arguments, we find it possible that in several cases a combination of ejecta and their interaction with high-speed stream possibly enhanced geomagnetic activity at or near the time of the passage of the ejecta. This appears to be the case for our events, numbered 3, 4, 9 and 12. In the case of Event 2, the high speed stream ahead of the ejecta also appears consistent with its possible source region near the equatorward boundary of a south-pole magnetic hole. Although no ejecta is observed in association with the 9 March 1997 H-CME (Webb et al., 2000b), at its expected time of arrival, the solar wind parameters show the possible remnants of a stream-stream interaction resulting from a repeat passage, 12–14 March, of a weakened equatorial extension of a south-pole magnetic coronal hole (Figs. 1b and 3 in Watari and Watanabe, 1998). Our Event 4 is also discussed in detail by Watari and Watanabe and they present convincing arguments to explain the fact that the ejecta appears to be overtaking the corotating high-speed stream. Finally, it is intriguing to find that in Event 5 the high-speed region near the reverse shock appears to be part of ejecta.

5.1 Ejecta and particle flow anisotropies

Anisotropy in the flux of energetic particles may allow for an independent test on the boundaries and extension of ejecta, usually interpreted as very large volumes with characteristic lengths in the $>$ 1000 Earth radii. In the case of cosmic rays Bieber and Evenson (1998) show for Event 3 (10–11 January 1997 IMC) unusual anisotropy in the flow of above 500 MeV particles. In general (at much lower energies), the presence of a bidirectional suprathermal particles flow along magnetic field lines may indicate the immersion of the observer in the ejecta domain of closed field lines, either connected to themselves or to the Sun (see, e.g. Gosling et al., 1990; Montgomery et al., 1974). In a recent study Shodhan et al. (2000) investigated the absence and or presence of bidirectional suprathermal electrons for IMCs observed by IMP-8 and Wind. In their analysis, they include several time intervals which are part of this study. In this case, we focus on the subset of events that overlap with ours. For these intervals, Shodhan et al. (2000) find substantial counterstreaming electrons for the long duration $\boldsymbol{B}$-field slow rotation intervals observed in Events 4, 6, 11, 13, and 14 of this paper. Shodhan et al. (2000) find a more sporadic presence of counter-

Table 4. Transit times, transit velocities and at 1AU evaluated velocities

	Transit Times [hr]			Velocities [kms^{-1}] (GSE)[d]					
Event	Shock-CME	EjLE[a]-CME	EjMP[b]-CME	Vsh		V(EjLE)		V(EjMP)	
				Vtr[c]	Vx(1 AU)	Vtr	Vx(1 AU)	Vtr	Vx(1 AU)
1	no shock	70.4	86.2?	–	–	−588	−470	−480	−408
2	no shock	94.3	121.4	–	–	−439	−420	−341	−337
3	79.4	83.6	94.5	−522	−439	−495	−460	−438	−440
4††	58.3	69.4	80.5	−710	−632	−596	−600	−514	−520†††
March†	no shock	no ejecta?	no ejecta?	–	–	–	–	–	–
5††	70.4	87.3	94.1	−588	−359	−474	−460	−440	−470
6	no shock	124.7	144.2	–	–	−332	−390	−287	−360
9††	65.75	69.4	82.1	−630	−422	−596	−440	−504	−468
10	103.2	108.9	128.9	−397	−339	−380	−350	−321	−316
June†	no shock	108±12	125±12	–	–	−383	−370	−330	−365
11	no shock	101.7	111.9	–	–	−407	−470	−370	−404
12	93.17	107.5	112.5	−444	−379	−385	−410	−368	−413
13	79.7	87.1	107.5	−520	−437	−475	−460	−385	−414
14	75.2	87.0	102.4	−551	−488	−476	−485?	−404	−453
mean	78.7	92.3	107.0	−545	−437	−463	−445	−413	−398

†) Events incorporated in the discussion (Sect. 5). [a]) EjLE = ejecta leading edge; [b]) EjMP = ejecta mid point, see convention in Sect. 5; [c]) Vtr = 1 AU divided by transit time, expressed in GSE coordinate convention; [d]) Velocity at 1 AU.
††) For completeness we mention that Metric Type II velocities for Events 4, 5, and 9 are, respectively, 600, 800, and 1400 km/s, taken from Smith et al. (2000). (For each event, the plane of the sky CME velocity is listed in column 3 in Table 2).
†††) See Appendix for Event 4 evaluation of the ejecta mid-point velocity.

streaming field-aligned electrons in corresponding intervals of Events 2 and 3 and a negligible presence in Event 9, while Events 1, 5, 10, and 12 were not part of their study. Since there is neither perfect overlap between their events and ours in the respective time extensions, nor in the event sets, we decided to redo the analysis of the suprathermal electron flow.

Our analysis confirms the findings by Shodhan et al. (2000) with no added time periods of counterstreaming electrons in Events 2, 3, 6, 11, and 14. This is not the case in Event 4, where suprathermal bidirectional electrons extend from 18:00 UT on 9 February to 04:00 UT on 12 February, well beyond the magnetic cloud-like interval. Counterstreaming electrons in this event overlap well with low $Tp/T_{\rm expected}$ throughout the interval and also cover isolated periods of above average $N\alpha/Np\%$ (see corresponding panels in Fig. 6B and entry in Table 3). Suprathermal bidirectional electrons are also identified in Event 5 from 22:30 UT on 10 April to 04:00 UT on 11 April and from 19:00 to 23:00 UT on 11 April. This later ejecta-interval contains a fast reverse interplanetary shock (Berdichevsky et al., 2000). For the magnetic cloud-like ejecta interval between 05:00 and 19:00 UT on 11 April (Fig. 6B, Table 3), the presence of bidirectional electrons is undetermined due to a loss of particle sampling during a long duration northward excursion of the $\boldsymbol{B}$-field (orientations which the Wind/SWE electron instrument cannot reach). In Event 9, suprathermal counterstreaming electrons are observed between 05:00 and 07:30 UT on 15 May, before the start of IMC. This short time interval in Event 9 shows good overlap with the similar interval of above average $N\alpha/Np\%$ ($\leq$ 10%). In Event 10, suprathermal bidirectional electrons are observed between 16:00 and 20:00 UT on 26 May, and near 10:00 UT on 27 May. Here again, between 20:00 and 24:00 UT on 26 May, there is no sampling due to high latitude excursion of the $\boldsymbol{B}$-field. Counterstreaming electrons are also found in Events 1 and 14, but there is almost a permanent connection with the bow shock, and in Event 1, it is not possible to disentangle one source from the other.

Suprathermal bidirectional electron streaming and composition (unusual solar wind $N\alpha/Np\%$) signatures combined to suggest that in Events 4, 5, and 9, ejecta passage started earlier and lasted longer than estimates that used solely IMC signatures, which combine the simultaneous observation of strong $\boldsymbol{B}$-field, low proton temperature and slow change in the orientation of the magnetic field.

5.2 Ejecta and Forbush decreases

Very energetic particle fluxes ($>$ 50 MeV proton observations with IMP-8, cosmic rays) should show a reduction in intensity when the Earth enters extended closed field regions. These Forbush decreases (Forbush, 1938, 1939) and related sudden decreases in the flow of several MeV energetic particles constitute another independent test of the passage of ejecta by Earth. A comparison with Table 1 in Cane et al. (1998), shows that Forbush decreases indicate the passage of ejecta for Events 4, 5, 9, and 10. This is also the case in

Event 2 (Farrugia et al., 2000), and in Events 11, 12, and 14, with weak Forbush decreases for Event 6 and no decreases in Events 1, 3, and 13 (I. G. Richardson, private communication, March 2001). This effect is not limited to the many MeV per nucleon energetic ions. Figures 5a and b show decreases in the flux of 2 MeV EP when entering cloud-like magnetic regions in those cases when their fluxes were above background. This is consistent with the Forbush decreases in Events 4, 5, and 9, but is also observed in Events 1 and 14 and it is possibly present in Events 6 and 10. In Event 2, there is a possible hindrance in MeV EP related to a new solar CME occurring during the IMC passage. Forbush decreases, when observed, were consistent with the start of magnetic cloud-like intervals, usually at a magnetic discontinuity.

5.3 Transit times of the driven IP shocks

Studies of the transit time of the driven shock versus the CME observed velocity appeared indicative of a deceleration of the shock (see, e.g. Cane et al., 1986). However, no deceleration was reported in the case of multiple spacecraft observations of six moderately strong shocks between ~ 0.7 and 1.0 AU (Mihalov et al., 1987).

Here we look at comparisons between shock transit times and the locally measured velocity of the shock (Table 4). For each event in the discussion, Table 4 presents Sun-Earth transit times and velocities for shocks and ejecta in columns 2 through 4, and 5 through 10, respectively. To distinguish it from its initial value near the Sun, we define a final shock velocity $Vf = Vx(1\,\mathrm{AU})$ as the local measurement of the shock velocity at 1 AU. These Vf allow us to test if their values are consistent with the shocks being driven by the ejecta. (Vf is from Berdichevsky et al., 2000, for those shocks observed before June 1997.) Table 4 shows that in seven cases the shock velocity matched within $\pm 30\,\mathrm{km}^{-1}$ the velocity of the ejecta leading edge. These differences are within the range of a typical solar wind Alvénic velocity. This is consistent with the interpretation that these shocks were still being driven by the ejecta, observed between 4–14 h behind the shock, as illustrated in Fig. 5. In all cases, Fig. 10 shows a shorter transit time (t) of the shock between Sun and Earth than the one suggested by the computed shock velocity. The mean difference is approximately $100\,\mathrm{km}^{-1}$ (see bottom row in columns 5 and 6 in Table 4). Assuming for calculation purposes constant acceleration, a, along the Sun-Earth line, we have

$$a = 2(Vf - Vtr)/t$$

with t, Vtr, and Vf being, respectively, the transit time from two solar radii to 1 AU, the transit velocity, and the locally measured shock velocity. In this way, it is possible to evaluate an effective change in speed of the shock between the Sun and the Earth. From the bottom row in Table 4, we obtain mean t, and $Vtr = 1\,\mathrm{AU}/t$. We find, in this way, a resulting effective mean initial velocity $Vi = Vtr + (Vtr - Vf)$ for the shock. This is about 200 ± 100 km/s faster closer to the Sun, than at 1 AU.

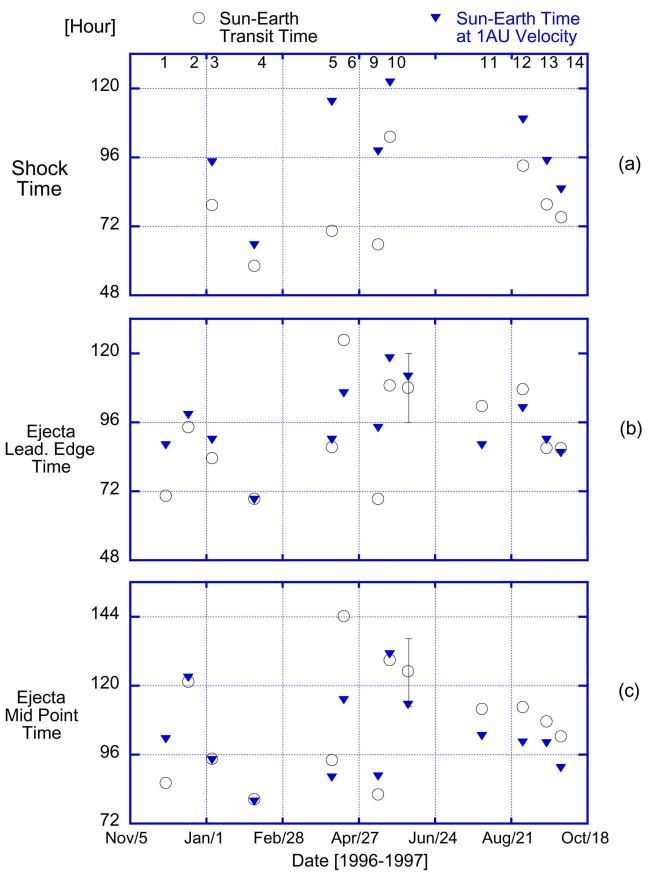

Fig. 10. For the events in Table 4 numbers at the top of panel **(a)** identify the event. Panel (a) shows shock transit times (open circle) and transit times for the estimated X_{GSE} component of the shock velocity (inverted solid triangle). Panel **(b)** shows transit times of the leading edge of the ejecta (open circle) and the corresponding estimate using its velocity along the Sun-Earth line (X_{GSE} direction). Panel **(c)** shows transit time of the middle point of the ejecta (open circle) and the corresponding estimate using the velocity, along X_{GSE}, of the ejecta mid-point (inverted solid triangle). The bar for Event 9 in panels (b) and (c) indicate approximate uncertainty in the evaluation of the transit velocities due to uncertainties at Sun and 1 AU on the identification of the H-CME and ejecta times, and ejecta velocity.

In the case of solar wind conditions covering Event 5 (10–11 April 1997), there is a large discrepancy in the speeds between shock (at 12:55 UT on 10 April) and the ejecta leading edge ($\sim$ 05:00 UT on 11 April). In addition the strong orientation of the shock away from the Sun-Earth line (Berdichevsky et al., 2000) supports the possibility of an extremely lateral shock encounter, as proposed in Berdichevsky et al. (1998). This would suggest two or more ejecta moving away from the Sun, consistent with decametric Type II radio emissions in association to the H-CME on 7 April 1997 (see Kaiser et al., 1998).

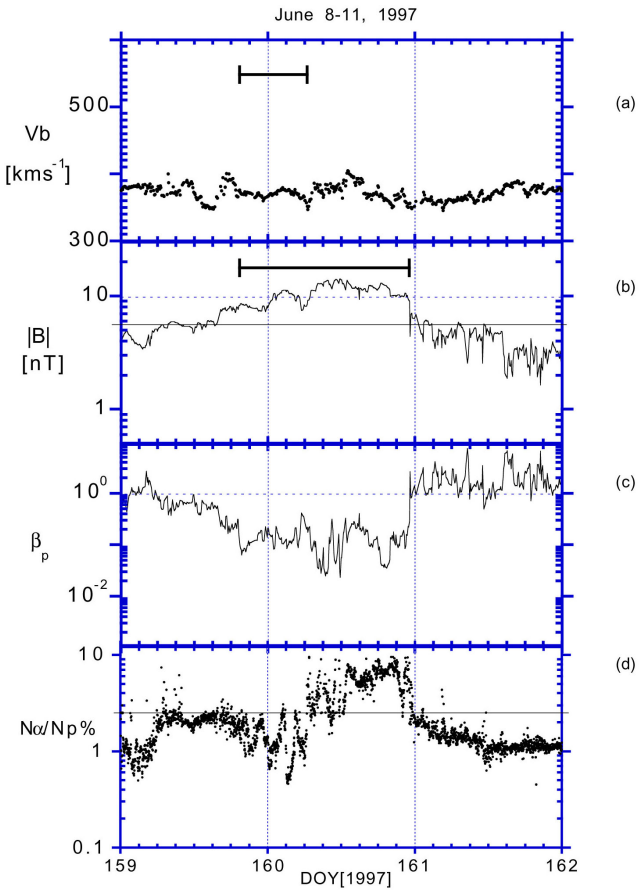

Fig. 11. The same as Figs. 6, for 8–11 June 1997

5.4 H-CME speed at two solar radii and 1 AU

Table 4 lists transit times in hours from the observation of the CME in the coronagraph C2 (Table 2) to the time of the passage by Wind of the mid-point of each ejecta (see Table 3). These are transit times of the ejecta mid-point ($EjMP$) taken as the center of the large magnetic field structure with a slow rotation in the orientation of the interplanetary magnetic field. A comparison of the corresponding transit velocity $Vtr(EjMP)$ to the Sun-Earth component of the solar wind velocity at ejecta mid-point $Vx(EjMP)$ shows a disagreement between average Vtr and $V(EjMP)$ of $\sim 15\,\mathrm{km}^{-1}$ (bottom row, columns 9 and 10 in Table 4). This difference in Table 4, near the $\sim 2\%$ uncertainty in the determination of solar wind velocities, indicates that at 1 AU the average ejecta is moving with mean velocity close to its estimated transit speed. This suggests at most a small change in the velocity of these ejecta, as a whole, from Sun to Earth. Similar is the difference between the average in situ Sun-Earth velocity of the ejecta leading-edge and its Vtr (columns 7 and 8, bottom, in Table 4). Translated into times (Sun-Earth distance divided by the transit velocities), this result is shown in Fig. 10 for each individual event listed in Table 4. It shows, for 12–15 May 1997 tracked Event 9, a 6 h increase in time for the Sun-Earth travel of ejecta mid-point, using its in situ velocity, than the actual transit time. The same times (i.e. $Vtr(EjMP) \approx Vx(EjMP)$) occur for the outcome of the 6–10 January 1997 tracked Event 3. Figure 10 shows that the mean values for both times in some cases agree and in others, their disagreements are less than half the mean time passage of the ejecta. This is not the case for the Sun-Earth connection candidate on 16–21 April 1997, Event 6, and the questionable 2–5 December 1996, Event 1. Event 6 appears to have an overly long transit time, corresponding to a realistic but locally unsupported transit speed of $\sim 290\,\mathrm{km}^{-1}$ (Table 4). In this case, two different conclusions could be drawn; (a) source misidentification, (b) substantial speed increase along its way from Sun to Earth. Smaller disagreements, larger than the uncertainty between transit time and travel time based on in situ velocity of the ejecta mid-point ($EjMP$) in Fig. 10 are present in Events 11 to 14, suggesting a small increase in their velocity from launch to passage by 1 AU.

The ejecta mid-point choice, for these comparisons, corresponds to a simple ballistic interpretation of the propagation of the center of mass of an isolated structure undergoing expansion and subjected to applied forces with an average resultant value equal to zero over the time of its transit from Sun to Earth. This could be considered a gross oversimplification; however, it should be valid for magnetic structures of plasma and field strength several times the surrounding solar wind environment. The local measurement of the solar wind velocity time series during the passage of the IMC corresponding to Event 9 appears to violate the above assumption, suggesting that this ejecta is subjected to strong nonzero force by a passing high-speed stream. However, Fig. 10 shows that the observed perturbations appear to have a small impact on the Sun-Earth transit time estimate of its midpoint, while larger disagreements are found between transit time and local velocity of front and rear ends of this ejecta (see corresponding velocity profile in top panel, Fig. 6C).

The evidence presented above concerning the center of the ejecta being convected at approximately constant speed between two solar radii and 1 AU is consistent with multispacecraft case studies of IMCs (between 0.3 and 5 AU by Osherovich, et al., 1993, and between 1 and 5 AU by Skoug et al., 2000). This finding between two solar radii and 1 AU appears to be confirmed recently for faster ejecta (Lepping et al., 2001a, b) possibly forcing reinterpretation of the statistical analysis in Gopalswamy et al. (2000).

5.5 Other ejecta, with unaccounted H-CME

It is possible that for some ejecta intervals encountered at 1 AU, there was no identification of H-CME at the Sun. If the ejecta velocity analysis for 16–21 April 1997 in Sect. 5.4 is interpreted as a case when the Sun source is misidentified, it adds to ejecta passages by Earth unrelated to H-CME. (This Event 6 could not be related to a later CME because there is no identification of CMEs after 07:35 UT 16 April and until 19:45 UT on 20 April 1997, in the report listed in file 1997.04_CME_List.txt reachable

from the LASCO/SOHO WEB page with URL: http://lasco-www.nrl.navy.mil/cmelist.html)

A strong case for an ejecta unrelated to H-CME is the case of the IMC observed on 8–9 June 1997. This event is reported by Brueckner et al. (1998), Webb et al. (2000b), and Shodahn et al. (2000). The observations at 1 AU are illustrated in Fig. 11. These local solar wind observations in Fig. 11 indicate that this event combines all characteristics found to be typical of ejecta, i.e. it has above average $\boldsymbol{B}$-field intensity. The $\boldsymbol{B}$-field shows a slow rotation over an extended interval and it was possible to fit using the force free model of Lundquist (Lepping et al., 1999). There are bidirectional streaming electrons and an above average $N\alpha/Np\%$ in its rear region. The assumption of a transit time corresponding to the velocity of the mid-point of the $\boldsymbol{B}$-field's slowly rotating interval put the lift-off time on 4 June. Indeed, on 4 June LASCO/SOHO observations indicate an unusual, continuous mass out-flow lasting almost a whole day. These slow outflows may be the result of filament eruption, supported by the EUV observation of arcade formation $\sim$14:00 UT on 3 June, near E 7° S 31° (AR8048). Consistent with time and location of these EUV observations is a report of the disappearance of two dark filaments in optical Hα-light on 3 June 1997 (*Solar Bulletin*). (The corresponding Sun-Earth times with a 12-h uncertainty are included in Table 4, and Fig. 10. They also show that for the 3–9 June 1997 Event $Vtr(EjMP) \approx Vx(EjMP)$).

6 Conclusions

The events presented in the analysis correspond to the near solar minimum epoch. They were selected on the basis of observation of H-CMEs, and their implication for Sun-Earth connections is investigated for those H-CMEs spaced three or more days in time.

It is found that in every case the ejection appears connected to a filament or prominence eruption. It is shown that good clear EUV sun disk signatures of the events are present in most cases. An EIT-wave was easier to note for AR ejecta. Filament eruption was observed in the non-AR eruptions. These EUV signatures appear to organize the ejections naturally into two categories; (a) AR related; (b) non-AR or a decayed AR. The investigated AR related H-CME showed transient chromospheric and low corona manifestations starting within approximately 180 min of the observation of the leading edge of the H-CME at two solar radii. Far longer times between filament eruption and observation of the H-CME at two solar radii are suggested by the observations in the case of non-AR ejections or filament eruptions from regions close to or related to decayed AR. In most AR related lift-offs, short wavelength radio emissions and other near-chromospheric signatures related to the ejection were reported. In contradistinction, less appeared to be reported for non-AR ejecta lift-off.

For six of the twelve fully discussed cases (50%), a shock driven in the inner heliosphere appeared to exist, being inferred through MeV ions and/or kilometric radio emisions. Two-thirds of them were related to eruption at/near AR and the other two were related to eruptions unrelated to AR. But there were more in situ shock observations with one case when inference of the shock in the inner heliosphere may have failed due to above average background levels in MeV EP. In seven cases, the in situ fast forward shock velocities matched the velocity of the leading edge of the identified ejecta interval, suggesting that they continued to be driven locally by the ejecta candidate. The transit times of these driven shocks, from the time of the H-CME to the time of its passage at 1 AU, suggested a deceleration of the shock. This deceleration observed amounts to a mean reduction in shock speed of $200 \pm 100\,\mathrm{km}^{-1}$ between Sun and Earth.

No single unifying indicator of an ejecta interval – which is divide into two classes: long lasting changes (a) in plasma parameters and (b) in the flow of EP – were identified, and this is consistent with findings by other works. The observed signatures, when existing, appeared downstream of the possibly driven shock and in all cases, within three to six days after the H-CME. (Notice that faster events have been observed close to solar maximum, e.g. Lepping et al., 2001a). Henceforth, ejecta were identified by the consistent overlap of the selected set of signatures, and we found that in two out of thirteen cases, ejecta indicators were lacking or absent, and these were H-CME related to source locations more than 60° W in longitude. All other cases appeared to have at least three or more consistent signatures of ejecta. They corresponded to ejecta with candidate solar disk sources within approximately 30° E or W from the solar central meridian, but within larger angular latitudinal extensions, in one case up to $\sim$ 50° N from ecliptic plane. The most commonly observed ejecta signatures in this set of events were found in a long lasting interval of plasma having low proton beta (ratio of the local plasma proton kinetic to magnetic field energy) and the slow rotation of the magnetic field vector. In seven cases, these intervals overlapped with identified IMCs, while two other cases overlapped with cloud-like intervals when the slow rotation of the field was not large enough for its unambiguous fit with the force free Lundquist model (Lundquist, 1950). (Hence, IMC were between $\approx$ 50 and 70% of the fully investigated cases.) In four cases, it appeared that the ejecta interval start and end times contain IMC or cloud-like intervals. In two of those cases, the synchronized observation of composition, flux-anisotropy, and the matching of shock velocity to the local observed solar wind combined to infer the start of the ejecta before the observation of the IMC or cloud-like part of the ejecta. In contradistinction, for two other cases, consistent signatures of ejecta started and ended with the identified IMC interval.

The mean passage duration of ejecta appeared to be above 33 h. When limiting passage time of the ejecta to the largest associated $\boldsymbol{B}$-field slow rotation region, the mean time became 24 h. This time is very close to the mean average time passage of IMCs (see, e.g. Lepping and Berdichevsky, 2000). These more ordered field and plasma intervals showed in all but one case a central velocity component along the Sun-

Table A1. IP shock and candidate ejecta intervals at 1 AU with temporal association with the 7 February 1997 H-CME

Time at 1 AU	Vel at 1 AU kms^{-1}	Start Time at the Sun Assuming Constant Velocity
12:55 UT, 9 Feb, IP S	632	14:14 UT, 6 Feb
02:00 UT, 10 Feb	570	01:12 UT, 7 Feb
18:00 UT, 10 Feb	500	05:40 UT, 7 Feb
21:00 UT, 11 Feb‡	390	02:12 UT, 7 Feb
04:00 UT, 12 Feb	370	03:30 UT, 7 Feb

‡Interval identified as associated to the H-CME prominence (Gopalswamy et al., 1998)

Earth direction, which, when assumed constant, projected back its lift-off time to the approximate observation of the halo-CME at two solar radii. This remarkable result has also been found for faster IMCs (Lepping et al., 2001a, b).

This paper did not attack the question "Is every ejecta at 1 AU the result of an observed CME (halo-CME)?" Nevertheless, it is interesting to note that possibly a few medium size ejecta may not have been observed as a CME or Halo-CME; this appears to be the case of the June 1997 event (see, e.g. Brueckner et al., 1998). And the discussion on transit times raises the possibility of having misidentified the source of 21–23 April ejecta. This non-exhaustive list would suggest that for every seven to ten observed H-CME, there is the possibility of one or two small to medium-sized unaccounted ejections, capable of causing a moderate geomagnetic storm, as was the case on 9 June and possibly on 21–23 April (both in 1997). Finally, in some cases (e.g. 20:00–23:00 UT 11 April, and 06:00–14:00 UT 16 May 1997), Figs. 6A–D show the presence of unusual solar wind conditions, possibly ejecta moving faster than earlier interval(s) that passed all necessary Sun-Earth connection conditions. These observations raise questions, beyond the scope of the present study, on the nature of these trailing intervals, their solar source, and their relationship to the earlier observed ejecta.

Appendix A Event 9 (12–16 May 1997)

On 12 May, images in the 195 Å line show that, between 04:50 and 05:41 UT, a EIT wave expanded over the whole solar disk from a location 6.5° W and 22° N (Thompson et al., 1998). 1–8 Å soft X-ray flux peaks at 04:55 UT with an intensity of a C1.3 flare. EIT images show that dimming near the magnetic neutral line developed between 04:34 and 07:00 UT (see Fig. 4 in Thompson et al., 1998). The H-CME appear at 07:35 UT, and its leading edge had an apparent velocity of $\sim$260 km/s (Figs. 1–3 in Plunkett et al., 1998). Metric Types I, II, III, and IV radio emissions (Hudson et al., 1998), and MeV EPs are present. The tracking of drifting IP radio emissions is shown in Figs. 1a and 5b. In situ solar wind observations are shown in Fig. 6C (Event 9). The mid-location in time of the ejecta passed Wind at 18:00 $\pm$ 02:00 UT traveling at a mean velocity of 470 $\pm$ 30 km/s. If maintained to 1 AU, this would indicate that the transient lifted off the Sun at 01:45 $\pm$ 05:30 UT on 12 May. This timing is in agreement, within experimental uncertainty, with the transient signatures seen at the Sun (see above). This agreement provides a selfconsistency check on the identification of the transient at the Sun and its manifestations at 1 AU.

Appendix B Event 4 (7–11 February 1997)

On 7 February 1997, EIT 195 Å line images and ground-based radio data show that, between 01:30 and 03:30 UT, a long filament that extended from 49° W to 24° E and from 22° to 25° S disappeared (Gopalswamy et al., 1998). GOES observed very weak soft X-ray enhancements which peak at 23:00 UT on 6 February. This event shows above background decametric Type III radio emissions. There is a delayed rise of the MeV EPs. There is a decrease in the MeV EP fluxes from approximately 18:00 UT 7 February to 22:00 UT 8 February, suggesting that EP fluxes are excluded from the closed field line region of an ejecta. The steady decline in EP fluxes ends near 04:00 UT on 9 February, and a spike in these fluxes at the time of the IP shock is suggested by the data in the 8–9.6 MeV He^{++} channel. Figure 6B shows that this transient candidate interval at 1 AU is preceded by a high-speed solar wind. The intensity of the MeV EP fluxes appear to be strongly suppressed between $\sim$04:00–20:00 UT on 10 February. This corresponds to the time interval when very low plasma densities ($Np < 1\,cm^{-3}$) and above average magnetic field strengths are observed by Wind (Fig. 6B, Event 4). From 03:00 UT to 18:00 UT, $\beta_p < 0.1$. From the start of 10 February until $\sim$21:00 UT, He^{++}/H^{+} is generally higher than in the surrounding time intervals, and lower than average for the period 03:00–06:00 UT, when a steady value of $\sim$1% is measured. Again, on 12 February, the solar wind shows above average He^{++}/H^{+} ratios, during an interval of below average solar wind speed and magnetic field strength. These observations at 1 AU suggest that the transient may have undergone strong modification due to its interaction with the observed fast stream. Since the densities are near zero from 04:00 to 20:00 UT on 10 February, the momentum flux is hard to estimate. In searching for the start of the event in the low corona, we look at the more dense individual regions of high He^{++}/H^{+} ratios. Table A1 presents the "back-at-the-Sun" lift-off times of transient material, assuming that each of the observed intervals of above average He^{++}/H^{+} propagate at the velocity measured at 1 AU.

The transit from Sun to Earth of all intervals shown in Table A1 indicates that each is a possible manifestation of the large filament eruption that took place on the Sun at 02:07 UT on 7 February. However, the IP shock arrives at 12:55 UT, on 9 February, with a measured local speed of $\sim$630 km/s (see Berdichevsky et al., 2000), and a travel-time indicative of a transit velocity of $\sim$720 km/s. This implies that the IP shock decreases its speed by $\sim$200 km/s between the Sun and the

Earth, an inference which is consistent with a possible weakening of shock strength manifested by the decline in intensity of MeV EP fluxes (Fig. 5a, Event 4). The longitude and latitude of the shock normal are $210 \pm 1°$, and $-20 \pm 2°$, respectively (Berdichevsky et al., 2000), which further suggests that more than 12 hours ahead of the observations at Wind on 9 February, we may see the eastern flank of the IP shock. In summary, these are observations that suggest the arrival at 1 AU of a "complex" ejecta, with a passage lasting from 9–12 February. In some respects, a similar case occurred on April 1997, described in Appendix C.

Appendix C Event 5 (7–11 April 1997)

For this event, disturbances on the solar disk started at about 13:27 UT, when a C6.8 flare went off. SOHO captures signatures of a EIT-wave in the low corona starting at $\sim$ 14:06 UT (Thompson et al., 1999). (This event shows one of the most intense and structured H-CMEs observed with LASCO/SOHO, with the leading edge of the CME appearing at 14:27 UT at 2 R_s from the Sun (e.g. Berdichevsky et al., 1998.) EIT images show clear signatures of dimming and arcade formation near the neutral line (bottom panels in Plate I).

Decametric drifting radio emissions are observed from the start of the event ($\sim$ 14:00 UT), and enhanced MeV EP a few hours later. It is apparent that drifting radio emissions were related to two possible shocks (Kaiser et al., 1998). The short-lived, drifting radio emissions appear to indicate a shock moving at twice the speed of the leading edge of the southeast concave structure ($\sim$ 840 km/s), possibly associated with the H-CME. The profile of the enhanced MeV EP fluxes suggests an origin close to central meridian, consistent with the location of the transient on the Sun ($\sim 19°$ E, Plate I, see, e.g. Richardson and Cane, 1993), and it extends until the passage of the ejecta near Earth on 11 April 1997. MeV EP fluxes are partially suppressed from 15:00 UT, 8 April to 09:00 UT 9 April, suggesting the presence of ejecta closed field lines. The intensities of MeV EP fluxes decrease starting at 00:00 UT on 10 April. As argued by Berdichevsky et al. (1998), there are clear indications that signatures of at least two transients were observed at 1 AU.

From 05:50 to 15:00 UT on 11 April, this ejecta has an unusually strong magnetic field ($\sim$ 25 nT) and correspondingly, an extremely low β_p, of $\sim 10^{-2}$. During the same time interval, the ratio $He^{++}/H^{+} > 6\%$ (Fig. 6B). The bulk flow speed is nearly constant between 450 and 490 km^{-1}. Using 10:00 UT, 11 April as the mid-time of the transient and the mean radial speed for the interval of 464 ± 10 km/s, we obtain a lift-off time of 16:00 $\pm$ 02:00 UT on 7 April 1997. Within experimental error, this estimate is in good agreement with the solar observations. A puzzling faster moving region beyond the ejecta's rear end is observed. It contains a reverse shock (20:52 UT on 11 April), immersed in an ejecta-type region with a ratio $Na/Np \sim 6\%$ and bidirectional electrons (from $\sim$ 20:00 to 23:00 UT).

Acknowledgements. We very much acknowledge the support by Drs. Aurass (Postdam, Germany) and Prestage (Culgoora, Australia) for providing information on the observation of metric radio emissions prior to publication. This work greatly benefited through many helpful discussions with Dr. Burlaga. Further, one of us (DBB) is grateful to Drs. St. Cyr and Webb for useful discussions, and Dr. Acuña for his support and encouragement. Work at UNH was partially supported by NASA Grant NAG5-2834. JTS thanks MIT's WIND team lead by A. J. Lazarus for continuing support and collaboration. Work by JTS while at MIT was supported under the NASA WIND project contract NAG5-7359. Work by JTS at LANL was performed under the auspices of the DOE with NASA support under S-92694-F. Work by DBB, RPL, and CJF was partially supported under the LWS grant NAG5-10883. We greatly benefited from the resources provided by the ISTP/Science Planning and Operation Facility at NASA/Goddard Space Flight Center. This includes among others: list of candidate events in the Catalog of Preliminary Solar Wind Events, plots of solar wind key parameters and plots of the orbit of Wind. These materials are provided through public domain Web pages, with URL http://spof-www.gsfc.nasa.gov. Last but not least we want to express our thanks for the support of the SOHO/LASCO and EIT, and WIND/SWE, MFI, EPACT, and WAVES instrument teams. We also greatly benefited, in specific cases, of the analysis of publicly available Yohkoh/SXT thermal X-ray images, and SOHO/MDI magnetograms.

Topical Editor E. Antonucci thanks two referees for their help in evaluating this paper.

References

Acuña, M. H., Ogilvie, K. W., Baker, D. N., Curtis, S. A., Fairfield, D. H., and Misch, W. H.: The Global Geospace Science Program and its Investigations, Space Science Rev., 71, 5, 1995.

Berdichevsky, D., Bougeret, J.-L., Delaboudinière, J.-P., Fox, N., Kaiser, M., Lepping, R. P., Michels, D., Plunkett, S., Reames, D., Reiner, M., Richardson, I., Rostoker, G., Steinberg, J., Thompson, B., and von Rosenvinge, T.: Evidence for multiple ejecta; April 7–11, 1997 ISTP Sun-Earth Connection Event, Geophys. Res. Lett., 25, 2473–2476, 1998.

Berdichevsky, D. B., Szabo, A., Lepping, R.P., Viñas, A. F., and Mariani, F.: Interplanetary Fast Shocks and Associated Drivers Observed Through the Twenty-Third Solar Minimum by WIND Over Its First 2.5 Years, J. Geophys. Res., 105, 27 289–27 314, 2000.

Bieber, W. J. and Evenson, P.: CME geometry in relation to cosmic ray anisotropy, Geophys. Res. Lett., 25, 2955–2958, 1998.

Bougeret, J.-L., Kaiser, M. L., Kellogg, P. J., Manning, R., Goetz, K., Monson, S. J., Monge, N., Friel, L., Meetre, C. A., Perche, C., Sitruk, L., and Hoang, S.: Waves: the radio and plasma wave investigation on the Wind spacecraft, Spa. Sci. Rev., 71, 231–267, 1995.

Bougeret, J.-L., Zarka, P., Caroubalos, C., Karlicky, M., Leblanc, Y., Maroulis, D., Hillaris, A., Moussas, X., Alissandrakis, C. E., Dumas, G., and Perche, C.: Correction to "A shock associated (SA) radio Event and related phenomena observed from the base of the solar corona to 1 AU", Geophys. Res. Lett., 25, 4103, 1998.

Brueckner, G. E., Howard, R. A., Koomen, M. J., Korendyke, C. M., Michels, D. J., Moses, J. D., Socker, D. G., Dere, K. P., Lamy,

P. L., Bedford, D. K., and Eyles, C. J.: The large angle spectroscopic coronograph (LASCO), Solar Phys., 162, 357, 1995.

Brueckner, G. E., Delaboudinière, J.-P., Howard, R. A., Paswaters, S. E., St. Cyr, O. C., Schwenn, R., Lamy, P., Simnett, G. M., Thompson, B.J., and Wang, D.: Geomagnetic storms caused by coronal mass ejections (CMEs): March 1996 through June 1997, Geophys. Res. Lett., 25, 3019–3022, 1998.

Burlaga, L., Sittler, E., Mariani, F., and Schwenn, R.: Magnetic loop behind an IP shock: Voyager, Helios, and IMP-8 observations, J. Geophys. Res., 86, 6673–6684, 1981.

Burlaga, L. F.: Magnetic clouds and force-free fields with constant alpha, J. Geophys. Res., 93, 7217–7224, 1988.

Burlaga, L.: Interplanetary Magnetohydrodynamics, Oxford Univ. Press, New York, 1995.

Burlaga, L., Fitzenreiter, R., Lepping, R., Ogilvie, K., Szabo, A., Lazarus, A., Steinberg, J., Gloeckler, G., Howard, R., Michels, D., Farrugia, C., Lin, R. P., and Larson, D. E.: A magnetic cloud containing prominence material: January 1997, J. Geophys. Res., 103, 277, 1998.

Cane, H., Stone, R. G., Fainberg, J., Stewart, R. T., Steinberg, J.-L., and Hoang, H.: Radio evidence for shock acceleration of electrons in the solar corona, Geophys. Res. Lett., 8, 1285–1288, 1981.

Cane, H. V. and Stone, R. G.: Type II solar radio bursts, interplanetary shocks and energetic particle events, Astrophys. J., 282, 339, 1984.

Cane, H. V., Kahler, S. W., and Sheeley, Jr. N. R.: Interplanetary shocks preceded by solar filament eruptions, J. Geophys. Res., 91, 13 321–13 329, 1986.

Cane, H. V., Reames, D. V., and von Rosenvinge, T. T.: The role of interplanetary shocks in the longitude distribution of solar energetic particles, J. Geophys. Res., 93, 9555, 1988.

Cane, H. V., Richardson, I. G., and von Rosenvinge, T. T.: Cosmic ray decreases: 1964–1994, J. Geophys. Res., 101, 21 561–21 572, 1996.

Cane, H. V., Richardson, I. G., and St. Cyr, O. C.: The interplanetary Events of January–May, 1997 as inferred from energetic particle data, and their relationship with solar Events, Geophys. Res. Lett., 25, 2517–2520, 1998.

Delaboudinière, G. E., Artzner, J., Brunaud, J., Gabriel, A. H., Hochedez, J. F., Millier, F., Song, X. Y., Au, B., Dere, K. P., Howard, R. A., Kreplin, R., Michels, D. J., Moses, J. D., Defise, J. M., Jamar, C., Rochus, P., Chauvineau, J. P., Marioge, J. P., Neupert, R. C., Maucherat, A., Clette, F., Cugnon, P., and VanDessel, E. L.: EIT: Extreme-Ultraviolet Imaging Telescope for the Soho mission, in: The SOHO Mission, (Eds) Fleck, B., Domingo, V., and Poland, A. I., Solar Phys., 162, 291–312, 1995.

Farrugia, C. J., Burlaga, L. F., and Lepping, R. P.: Magnetic clouds and the quiet-storm effect at Earth, in: Magnetic Storms, (Eds) Tsurutani, B. T., Gonzalez, W. D., Kamide, Y., and Arballo, J. K., pp. 91, Geophys. Mono. Series, 98, AGU, 1997a.

Farrugia, C. J.: Recent work on modeling the global field line topology of IMC in coronal mass ejections, pp. 177–188, (Eds) Crooker, N., Jocelyn, J., and Feynman, J., Geophysical Monograph, 99, AGU, 1997b.

Farrugia, C. J., Vasquez, B. J., Torbert, R. B., Janoo, L., Richardson, I. G., Reiner, L. M., Berdichevsky, D., Burlaga, L. F., Ogilvie, K. W., Osherovich, V. A., Fitzenreiter, R. J., Szabo, A., and Lazarus, A. J.: Multi-instrument study of the December 1996 magnetic cloud and associated interplanetary disturbances, in The Solar Wind – Magnetosphere System-3, 99, Austrian Academy of Sciences, Austria, 2000.

Forbush, S. E.: On cosmic-ray effects associated with magnetic storms, Terr. Mag., 43, 203–218, 1938.

Forbush, S. E.: World-Wide Changes in Cosmic-Ray Intensity, Rev. Mod. Phys., 11, 168–172, 1939.

Goldstein, R., Neugebauer, M., and Clay, D.: A statistical study of CME plasma flows, J. Geophys. Res., 103, 4761–4766, 1998.

Gopalswamy, N., Hanaoka, Y., Kosugi, T., Lepping, R. P., Steinberg, J. T., Plunkett, S., Howard, R. A., Thompson, B. J., Gurman, J., Ho, G., Nitta, N., and Hudson, H. S.: Geophys. Res. Lett., 25, 2485–2488, 1998.

Gopalswamy, N., Lara, A., Lepping, R. P., Kaiser, M. L., Berdichevsky, D., and St. Cyr, O. C.: Interplanetary acceleration of coronal mass ejections, Geophys. Res. Lett., 27, 145–148, 2000.

Gosling, J. T., Hildner, E., Macqueen, R. M., Munro, R. H., Poland, A. I., and Ross, C. L.: Mass ejections from the sun: a view from SKYLAB, J. Geophys. Res., 79, 4581, 1974.

Gosling, J. T.: Coronal mass ejections and magnetic flux ropes in interplanetary space, in: Physics of Magnetic Flux Ropes, Geophys. Monogr. Ser., Vol. 58, (Eds) Russell, C. T., Priest, E. R., and Lee, L. C., p. 343, AGU, Washington, D. C., 1990.

Hirshberg, J., Bame, S. J., and Robbins, D. E.: Solar flares and solar wind helium enrichments: July 1965–July 1967, Sol. Phys., 23, 467, 1972.

Hoang, S., Maksimovic, M., Bougeret, J.-L., Reiner, M. J., and Kaiser, M. L.: Wind-Ulysses source location of radio emissions associated with the January 1997 Coronal Mass Ejection, Geophys. Res. Lett., 25, 2497–2500, 1998.

Howard, R. A., Michels, D. J., Sheeley, Jr., N. R., and Koomen, M. J.: The observation of a Coronal Transient Directed at Earth, Astrophys. J., 263, L, 101–104, 1982.

Hudson, H. S., Lemen, J. R., St. Cyr, O. C., Sterling, A. C., and Webb, D. F.: X-ray coronal changes during halo CMEs, Geophys. Res. Let., 25, 2481–2484, 1998.

Joselyn, J. A. and McIntosh, P. S.: Disappearing Solar Filaments: A useful predictor of geomagnetic activity, J. Geophys. Res., 86, 4555–4564, 1981.

Kaiser, M. J., Reiner, M. J., Gopalswamy, N., Howard, R. A., and St. Cyr, O. C.: Type II radio emissions in the frequency range from 1–14 MHz associated with the 7 April 1997 solar Event, Geophys. Res. L., 25, 2501–2504, 1998.

Klein, L. W. and Burlaga, L. F.: Magnetic clouds at 1 AU, J. Geophys. Res., 87, 613–624, 1982.

Lengyel-Frey, D., Thejappa, G., MacDowall, R. J., Stone, R. G., and Phillips, J. L.: Ulysses observations of wave activity at interplanetary shocks and implications for Type II radio bursts, J. Geophys. Res., 102, 2611–2621, 1997.

Lepping, R. P., Acuña, M. H., Burlaga, L. F., Farrell, W. M., Slavin, J. A., Schatten, K. H., Mariani, F., Ness, N. F., Neubauer, F. M., Whang, Y. C., Byrnes, J. B., Kennon, R. S., Panetta, P. V., Scheifele, J., and Worley, E. M.: The WIND Magnetic Field Investigation, Space Science Rev., 71, 207–229, 1995.

Lepping, R. P., Berdichevsky, D., Szabo, A., Burlaga, L. F., Thompson, B. J., Mariani, F., and Lazarus, A. J.: Typical and Unusual Properties of Magnetic Clouds during the WIND Era, SH51A-08 abstract, EOS Transactions, AGU Spring Meeting, 80, p. S267, 1999.

Lepping, R. P. and Berdichevsky, D.: Interplanetary magnetic clouds: sources, properties, modeling, and geomagnetic relationship, Ed. Research Signpost, Vallakkadavu, India, Recent Research Developments in Geophysical Research, Vol. 3, 2000.

Lepping, R. P., Berdichevsky, D., Szabo, A., Lazarus, A.J., and

Thompson, B. J.: Upstream shccks and interplanetary magnetic cloud speed and expansion: Sun, Wind, and Earth observations, Adv. Space Res., 26, in press, 2001a.

Lepping, R. P., Berdichevsky, D. B., Burlaga, L. F., Lazarus, A. J., Kasper, J., Desch, M. D., Wu, C.-C., Reames, D. V., Singer, H. J., Smith, C. W., and Ackerson, K. L.: The Bastille day magnetic clouds and upstream shocks: Near Earth interplanetary observations, Solar Physics, in press, 2001b.

Lopez, R. E.: Solar cycle invariance in solar wind proton temperature relationships, J. Geophys. Res., 92, 11 189, 1987.

Lopez R. E. and Freeman, J. W.: The solar wind proton temperature-velocity relation, J. Geophys. Res., 91, 1701, 1986.

Lundquist, S.: Magnetohydrostatic fields, Ark. Fys., 2, 361, 1950.

Martin, S.: The evolution of prominences and their relation to active centers, Sol. Phys., 31, 3, 1973.

Marubashi, K.: Structure of the interplanetary magnetic clouds and their solar origins, Adv. Space Res., 6, 335–338, 1986.

Michels D. J.: Organization of the corona at solar minimum, in: Proceedings of the Third Soltip Symposium, Oct. 14–18, 1996, Beijing, China, (Eds) Feng X. S., Wei F. S., and Dryer M., Printed by the Int. Acad. Publs., Beijing, China, Plates 1–5, and pp. 34–39, 1998.

Mihalov, J. D., Russell, C. T., Knudsen, W. C., and Scarf, F. L.: Pioneer, Venus and near-Earth observation of interplanetary shocks, J. Geophys. Res.,92, 3385–3391, 1987.

Mish, W. H., Green, J. L., Reph, M. G., and Peredo, M.: ISTP science data systems and products, Space Sci. Rev., 71, 815–878, 1995.

Montgomery, M. D., Asbridge, J. R., Bame, S. J., and Feldman, W. C.: Solar wind electron temperature depressions following some interplanetary shock waves, Evidence for magnetic merging?, J. Geophys. Res., 79, 3103–3110, 1974.

Munro, R. H., Gosling, J. T., Hildner, E., MacQueen, R. A., Poland, A. I., and Ross, C. L.: The association of coronal mass ejection transients with other forms of solar activity, Sol. Phys., 61, 201, 1979.

Neugebauer, M.: Observations of solar wind helium, Fundamentals of Cosmic Physics, 7, 131–199, 1981.

Neupert, W.: Transient coronal extreme ultraviolet emission before and during the impulsive phase of a solar flare, Ap. J., 304, 504–512, 1989.

Ogilvie, K. W., Chornay, D. J., Fitzenreiter, R. J., Hunsaker, F., Keller, J., Lobell, J. , Miller, G., Scudder, J. D., Sittler, E. C., Torbert, R. B., Bodet, D., Needell, G., Lazarus, A. J., Steinberg, J. T., Tappan, J. H., Mavretic, A., and Gergin, E.: SWE, A Comprehensive Plasma Instrument for the Wind Spacecraft, Space Science Rev., 71, 55–77, 1995.

Osherovich, V. A, Farrugia, C. J., and Burlaga, L. F.: Dynamics of aging magnetic clouds, Adv. Space Res. 13, 6(6), 57, 1993.

Pintér, S.: Relation between Moreton Waves, Type II Shocks and Interplanetary Shock Waves, Proceedings of COSPAR Symposium B, (Eds) Shea, M. A., Smart, D. F., and Wu, S. T., AGGL-TR-77-0309 Special Reports, No. 209, Tel Aviv, Israel, 1977.

Plunkett, S. P., Thompson, B. J., Howard, R. A., Michels, D. J., St. Cyr, O. C., Tappin, S. J., Schwenn, R., and Lamy, P. L.: LASCO observations of an Earth-directed coronal mass ejection on May 12, 1997, Geophys. Res., Lett., 25, 2477–2480, 1998.

Plunkett, S. P., Thompson, B. J., St. Cyr, O. C., and Howard, R. A.: Solar source regions of coronal mass ejections and their geomagnetic effects, J. Atmos. Solar-Terr. Phys., 63, 389–402, 2001.

Reames, D. V., Barbier, L. M., and Ng, C. K.: The spatial distribution of particles accelerated by coronal mass ejection-driven shocks, Astrophys. J., 466, 473–486, 1996.

Reiner, M. J., Kaiser, M. L., Fainberg, J., Bougeret, J.-L., and Stone, R. G.: On the origin of radio emissions associated with the January 6–11, 1997, CME, Geophys. Res. Lett., 25, 2493–2496, 1998a.

Reiner, M. J., Kaiser, M. L., Fainberg, J., and Stone, R. G.: A new method for studying remote type II radio emissions from coronal mass ejection-driven shocks, J. Geophys. Res., 103, 29 651–29 664, 1998b.

Richardson, I. G. and Cane, H. V.: Signatures of shock drivers in the solar wind and their dependence on the solar source location, J. Geophys. Res., 98, 15 295, 1993.

Richardson I. G. and Cane, H. V.: Regions of abnormally low proton temperature in the solar wind (1965–1991) and their association with ejecta, J. Geophys. Res., 100, 23 397, 1995.

Sanahuja, B., Domingo, V., Wenzel, K. P., Joselyn, J. A., and Kepler, E.: A large proton Event associated with solar filament activity, Solar Physics, 84, 321, 1983.

Sanderson, T. R., Lin, R. P., Larson, D. E., McCarthy, M. P., Parks, G. K., Bosqued, J. M., Lorman, N., Ogilvie, K., Lepping, R. P., Szabo, A., Lazarus, A. J., Steinberg, J. T., and Hoeksama, J. T.: Wind observations of the influence of the Sun's magnetif field on the interplanetary medium at 1 AU, J. Geophys. Res., 103, 17 235–17 247, 1998.

Sheeley, Jr., N. R., Wang, Y.-M., Hawley, S. H., Brueckner, G. E., Dere, K. P., Howard, R. A., Koomen, M. J., Korendyke, C. M., Michels, D. J., Paswaters, S. E., Socker, D. G., St. Cyr, O. C., Wang, D., Lamy, P. L., Llebaria, A., Schwenn, R., Simnett, G. M., Plunkett, S., and Biesecker, D. A.: Measurements of flow speeds in the corona between 2 and 30 solar radii, Astrophys. J., 484, 472–478, 1997.

Scherrer, P. H., Bogart, R., Bush, R., Hoeksema, J., Kosovichev, A., Schou, J., Rosenberg, W., Springer, L., Tarbell, T., Title, A., Wofson, C., Zayer, I., Akin, D., Carvalho, B., Chevalier, R., Duncan, D., Edwards, C., Katz, N., Levay, M., Lindgren, R., Mathur, D., Morrison, S. Pope, T., Rehse, R., and Torgeson, D.: The solar oscillations investigation – Michelson doppler imager, Sol. Phys., 162, 129–188, 1995.

Shodhan, S., Crooker, N. U., Kahler, S. W., Fitzenreiter, R. J., Larson, D. E., Lepping, R. P., Siscoe, G. L., and Gosling, J. T.: Counterstreaming electrons in magnetic clouds, J. Geophys. Res., 105, 27 261–27 268, 2000.

Skoug, R. M., Feldman, W. C., Gosling, J. T., McComas, D. J., Reisenfeld, D. B., Smith, C. W., Lepping, R. P., and Balogh, A.: Radial varation of solar wind electrons inside a magnetic cloud observed at 1 and 5 AU, J. Geophys. Res., 105, 27 269–27 275, 2000.

Smith, Z., Dryer, M., Ort, E., and Murtagh, W.: Performance of Interplanetary Shock Prediction Models: STOA and ISOM, J. Atmos. Solar-Terr. Phys., 62, 1265–1274, 2000.

St. Cyr, O. C. and Hundhausen, A. J.: On the interpretation of halo coronal mass ejections, Proc. Solar Wind VI Coference, (Eds) Pizzo, V. J., Holzer, T. E., and Sime, D. G., 235–241, 1988.

St. Cyr, O. C., Burkerpile, J. T., Hundhausen, A. J., and Lecinski, A. R.: A comparison of ground-based and spacecraft observations of CMEs from 1980–1989, J. Geophys. Res., 104, 12 493–12 506, 1999.

St. Cyr, O. C., Howard, R. A., Sheeley, N. R., Plunkett, S. P., Michels, D. J., Paswaters, S. E., Koomen, M. J., Simnett, G. M., Thompson, B. J., Gurman, J. B., Schwenn, R., Webb, D. F., Hildner, E., and Lamy, P. L.: Properties of coronal mass ejections: SOHO LASCO observations from January 1996 to June

1998, J. Geophys. Res., 105, 18 169–18 185, 2000.

Steinberg, J. T., Lazarus, A. J., Ogilvie, K. W., Lepping, R., and Byrnes, J.: Differential flow between solar wind protons and alpha particles: First WIND observations, Geophys. Res. Lett., 23, 1183–1186, 1996.

Thejappa, G., MacDowall, R. J., and Viñas, A. F.: In situ Wave Phenomena in the Upstream and Downstream regions of Interplanetary Shocks: Implications for Type II Burst Theories, In the Proceedings of ESLAB Symposium no. 13, in press, 1998.

Thompson, B. J., Plunkett, S. P., Gurman, J. B., Newmark, J. S., St. Cyr, O. C., and Michels, D. J.: SOHO/EIT observations of an Earth-directed coronal mass ejection on May 12, 1997, Geophys. Res. Lett., 25, 2465–1468, 1998.

Thompson, B. J., Newmark, J. S., Gurman, J. B., Neupert, W., Delaboudinière, J.-P., St. Cyr, O. C., Stezelberger, S., Dere, K. P., Howard, R. A., and Michels, D. J.: SOHO/EIT observations of the 7 April 1997 coronal transient: Possible Evidence for coronal Moreton waves, Astro. J. Letts., 517, L, 151–154, 1999a.

Thompson, B. J., St. Cyr, O. C., Plunkett, S. P., Gurman, J. B., Gopalswamy, N., Hudson, H. S., Howard, R. A., Michels, D. J., and Delaboudinière, J.-P.: The correspondence of EUV and white light observations of coronal mass ejections with SOHO EIT and LASCO, in: Sun-Earth Plasma Connections, Geophys. Monograph Ser., vol. 109, (Eds) Burch, J. L., Carovillano, R. L., and Antiochos, S. K., p. 31, AGU, Washington, D. C., 1999b.

Torsti, J., Anttila, A., Kocharov, L., Mäkelä, P., Riihonen, E., Sahla, T., Teittinen, M., Valtonen, E., Laitinen, T., and Vainio, R.: Energetic ($\sim$ 1 to 50 MeV) protons associated with Earth-directed coronal mass ejections, Geophys. Res. Lett., 25, 2525–2428, 1998.

Uchida, Y.: Propagation of hidromagnetic disturbances in the solar corona and Moreton's wave phenomenon, Solar Phys., 4, 30–44, 1968.

Uchida, Y., Altschuler, M. D., and Newkirk, G.: Flare-produced coronal MHD-fast-mode wavefronts and Moreton's wave phenomenon, Solar Phys., 28, 495–516, 1973.

von Rosenvinge, T. T., Barbier, L. M., Karsch, J., Liberman, R., Madden, M. P., Nolan, T., Reames, D. V., Ryan, L., Singh, S., Trexel, H., Winkert, G., Mason, G. M., Hamilton, D. C., and Walpole, P.: The energetic particles: acceleration, composition, and transport (EPACT) investigation on th eWind spacecraft, Spa. Science Rev., 71, 155–206, 1995.

Watari, S. and Watanabe, T.: The solar drivers of geomagnetic disturbances during solar minimum, Geophys. Res. Lett., 25, 2489–2492, 1998.

Webb, D. F., Cliver, E. W., Gopalswamy, N., Hudson, H. S., and St. Cyr, O. C.: The solar origin of the January 1997 coronal mass ejection, magnetic cloud and geomagnetic storm, Geophys. Res. Lett., 25, 2469–2472, 1998.

Webb, D. F., Cliver, E. W., Crooker, N. U., St. Cyr, O. C., and Thompson, B. J.: Relationship of halo coronal mass ejections, magnetic clouds, and magnetic storms, J. Geophys. Res., 105, 7491–7508, 2000a.

Webb, D. F., Lepping, R. P., Burlaga, L. F., DeForest, C. E., Larson, D. E., Martin, S. F., Plunkett, S. P., and Rust, D. M.: The origin and development of the May 1997 magnetic cloud, J. Geophys. Res., 105, 27 251–27 259, 2000b.

Zirin, H.: The solar atmosphere, (Ed) Blaisdell Publishing Co., Waltham, MA, 1966.

Zwickl, R. D., Asbridge, J. R., Bame, S. J., Feldman, W. C., Gosling, J. T., and Smith, E. J.: Plasma properties of driver gas following interplanetary shocks observed by ISEE-3, SOLAR WIND FIVE, NASA Conf. Publ., CP-2280, 711, 1983.